Chemie der Erde 78 (2018) 462–478

Contents lists available at ScienceDirect

Chemie der Erde

journal homepage: www.elsevier.com/locate/chemer

Iron oxide copper-gold (IOCG) mineralization at the Imiter inlier, Eastern Anti-Atlas, Morocco

Bouchra Baidada[a,*], Abdelkhalek Alansari[a], Basem Zoheir[b,c], Said Ilmen[d], Abderrahmane Soulaimani[a], Moha Ikenne[e]

[a] Department of Geology, Faculty of Sciences-Semlalia, Cadi Ayyad University, Prince Moulay Abdellah Boulevard, P.O. Box 2390, 40 000, Marrakech, Morocco
[b] Department of Geology, Faculty of Science, Benha University, 13518, Benha, Egypt
[c] Institute of Geosciences, Kiel University, Ludewig-Meyn Str. 10, 24118, Kiel, Germany
[d] Managem Group, Twin Center, 20 100, Casablanca, Morocco
[e] LAGAGE Laboratory, Department of Geology, Faculty of Sciences, Ibn Zohr University, P.O. Box 28/S, 80 000, Agadir, Morocco

ARTICLE INFO

Handling Editor: Astrid Holzheid

Keywords:
Bou Fliou IOCG deposit
Magnetite-hematite
Granodiorite
Geochemistry
Imiter inlier
Anti-Atlas
Morocco

ABSTRACT

The Imiter inlier at the eastern Anti-Atlas chain (Morocco) hosts a world-class epithermal Ag-Hg deposit, and several occurrences of sulfide-magnetite mineralization. These occurrences are confined to transcurrent faults that cut mildly to highly potassic I- and S-type granite intrusions (e.g., Igoudrane, Bou Teglimt, Taouzzakt and Bou Fliou).

In this contribution, we present new field, petrographic and microanalytical data of the Bou Fliou sulfide-magnetite mineralization in the northwestern part of the Bou Teglimt granodiorite intrusion (567 ± 6Ma). Field and microscopic investigations reveal pervasive silicification and potassic alteration associated with iron oxides-rich (> 10 vol %) veins, stockworks, and breccias along NE-SW faults. The ore minerals are mainly magnetite, hematite, chalcopyrite, pyrite, sphalerite, Ag-galena, cobaltite, and less abundant Bi-sulfosalts (i.e., cosalite, galenobistmuthite, and llilanite-gustavite). The low-titanium iron oxides (magnetite and hematite), widespread iron-rich breccia, association with crustal scale fault zone, pervasive alteration, and overprinting mineral assemblages suggest a shallow level IOCG-style mineralization. High-order splays of the major fault zone could have provided effective traps for magmatic and basinal Cu and Zn-Pb hydrothermal fluids. The ~550 Ma intrusive phases in the region could have contributed by fluid, elements or heat in a local effective blumbing. The mineralogical and ore textural criteria reflecting ore formation at a realtively shallow crustal environment, but a fluid inclusion study is needed to characterize the ore fluids and mechanism of ore deposition.

1. Introduction

The Pan-African belts of Africa have never been considered the first priority for mineral exploration in Archean, early Proterozoic and Phanerozoic terranes if assessed against their historical perspective of mineral exploration and production. However, recent advances in understanding of the evolution of Pan-African sequences and a number of recent exploration successes suggest that Pan-African terranes merit more attention than was previously afforded (e.g., Foster et al., 2001; Gasquet et al., 2008; Bouabdellah et al., 2016).

Iron oxide copper-gold deposits (IOCG) comprise a type of mineralization formed in the geological time scale, from the Archean to Phanerozoic with most important occurrences in Australia and South America but also in Africa (Nisbet et al., 2000; Williams et al., 2005). Generally, these deposits contain massive and disseminated iron oxides (magnetite and/or hematite) that are partially or completely replaced by sulfides, i.e., pyrite and chalcopyrite. The style of mineralization and geometry of the mineralized bodies vary from veins, stockworks to breccia pipes or replacement mantos as stratabound or discordant bodies (Hitzman et al., 1992). Commonly, the IOCG deposits lack a demonstrated intimate relationship to particular intrusive phases, but a few cases are associaty with intrusions showing similar geochemical features as those linked to the porphyry Cu–Au deposits (e.g., Pollard, 2000, 2006). The large occurrences of massive iron oxides in some IOCG deposits include: (a) a classical BIF ore, (b) hydrothermal replacement of granitoids, and (c) selective hydrothermal replacement of layered rocks (e.g., Barton and Johnson, 1996; Bastrakov et al., 2007; Monteiro et al., 2008).

* Corresponding author.
E-mail address: bouchrabaidada@gmail.com (B. Baidada).

https://doi.org/10.1016/j.chemer.2018.10.002
Received 8 August 2018; Received in revised form 28 September 2018; Accepted 1 October 2018

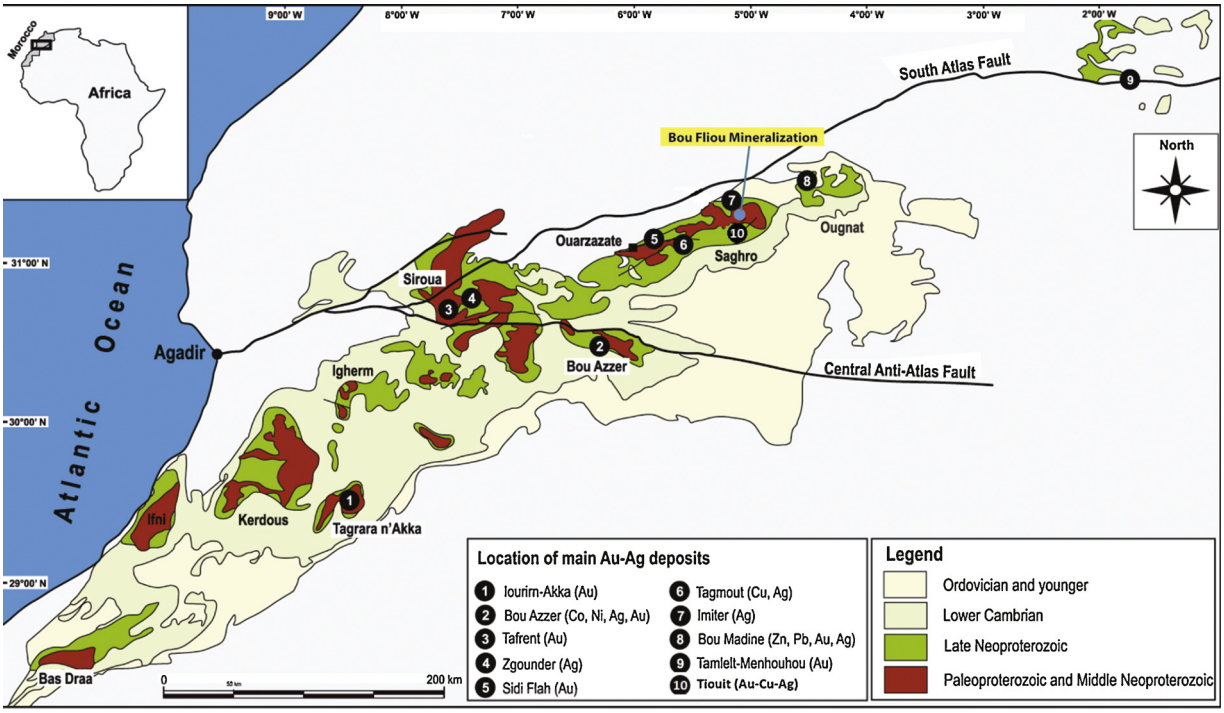

Fig. 1. Simplified geological map of the Anti-Atlas system showing location of the Bou Fliou mineralization and the main Au-Ag deposits (in Bouabdellah et al., 2016).

The Moroccan Eastern Anti-Atlas (Saghro massif) is a metallogenic province known for several occurrences of iron oxide-base metal deposits (Fig. 1). Several occurrences of massive and vein-type ploymetallic Cu-Au-Ag mineralization are located south of the Imiter world-class epithermal silver deposit (Levresse, 2001; Tuduri et al., 2005; Gaouzi et al., 2011; Essarraj et al., 2017) and north of the Tiouit porphyry deposit (Alansari, 1997; Alansari et al., 2011; Bouabdellah et al., 2016).

The recent recognition of iron oxide-polymetallic mineralization in close association with extensive metasomatism along major structures and local enrichment in light REE and Au in the Imiter inlier suggests a possible IOCG mineralization style in the Anti-Atlas, Saghro massif (e.g., Ehrig et al., 2013). In this contribution, field observations combined with mineralogical, geochemical and structural data of the Bou Fliou deposit in a genetic model, in which the setting and controls of the surrounding ore deposits (Imiter and Tiouit) are considered. Such a genetic model would help and promote exploration successes in this yet poorly-explored metallogenic belt.

2. Geological setting

2.1. Lithostratigraphy of the Imiter inlier

The Anti-Atlas belt is made up of two contrasting Precambrian domains separated by the WNW-ESE Anti-Atlas major fault, which crosscuts the Bou-Azzer, Siroua and northern Zenaga inliers (Gasquet et al., 2008 and references therein). The southwestern cratonic domain includes Paleoproterozoic gneisses and granites dated as 2 Ga (e.g., Bas Drâa, Kerdous, Ifni, Zenaga; Aït Malek et al., 1998; Walsh et al., 2002; Thomas et al., 2002; Gasquet et al., 2005; O'Connor et al., 2010; El Hadi et al., 2010; Soulaimani et al., 2014), while the central and eastern parts are Pan-African mobile belts (e.g., Gasquet et al., 2005; Walsh et al., 2012). The Imiter inlier is located at the eastern side of the Anti-Atlas fault and west of the Ougnat inlier (Fig. 2; Hindermeyer et al., 1977). In this inlier, the Saghro Group forms a triangular block of 1200 m-thick turbiditic flysch sediments intercalated with ~50 m-thick tholeiitic metabasalt sheets (Guillou et al., 1988; Leistel and Qadrouci, 1991; Ouguir et al., 1994; Barodi et al., 1998; Baroudi et al., 1999; Cheilletz et al., 2002; Fekkak et al., 2002; Levresse et al., 2004).

The Saghro group is subdivided into four units, namely: (i) a lower sandstone unit; (ii) a sandstone-pelitic intermediate unit; (iii) a pelitic unit; and (iv) an upper black shale unit (Schiavo et al., 2007). The turbiditic series of the Saghro Group are tightly folded around a NE-SW axial plane (Fig. 3). Strong schistosity and stretching lineations are common in the different units of the group.

2.2. Magmatic history

In the Imiter inlier, the Saghro Group is intruded by a set of medium-K calc-alkaline (BouTeglimt, Taouzzakt, BouFliou) and high-K calc-alkaline (Igoudrane) granitoid intrusions (Fig. 3; Camara, 1993; Errami et al., 2009; Baidada et al., 2017). Formation of these intrusions is thought to post-dating the regional deformation in the metasedimentary rocks (Guilllou et al., 1981, 1988). The Igoudrane and Bou Teglimt intrusions are, however, considered syn-tectonic to the Pan-African compressional deformation assigned as phase PA1. On the other hand, the Taouzzakt granodiorite is suggested to have formed in a post-tectonic within-plate environment (e.g., Grappe, 1974, Vargas, 1983; Ighid et al., 1989).

Zircon U-Pb SHRIMP data of the Imiter granitoids indicate their Ediacaran age (Walsh et al., 2012; Baidada et al., 2018). The Igoudrane massif was considered to be synchronous to the major Pan-African compressional deformation (e.g., Ighid et al., 1989), while the new ages obtained (Baidada et al., 2017) are significantly younger ages (540–575 ± 5 Ma) than the previousely published zircon U-Pb TIMS (677Ma; Schiavo et al., 2007).

The geodynamic models proposed for the Ediacaran magmatic series relate these rocks to the Pan-African orogenic events (Bajja, 1998; El Baghdadi et al., 2003; Benziane, 2007; Walsh et al., 2012; Hefferan et al., 2014; Baidada et al., 2018), or alternatively to a post-collisional collapse and subsequent asthenospheric rise beneath a reworked edge of the West African Craton (Thomas et al., 2002; Ennih and Liégeois, 2001, 2008; Gasquet et al., 2005, 2008). Toummite et al. (2012) suggested that the Ouarzazate Group was generated during the evolution of

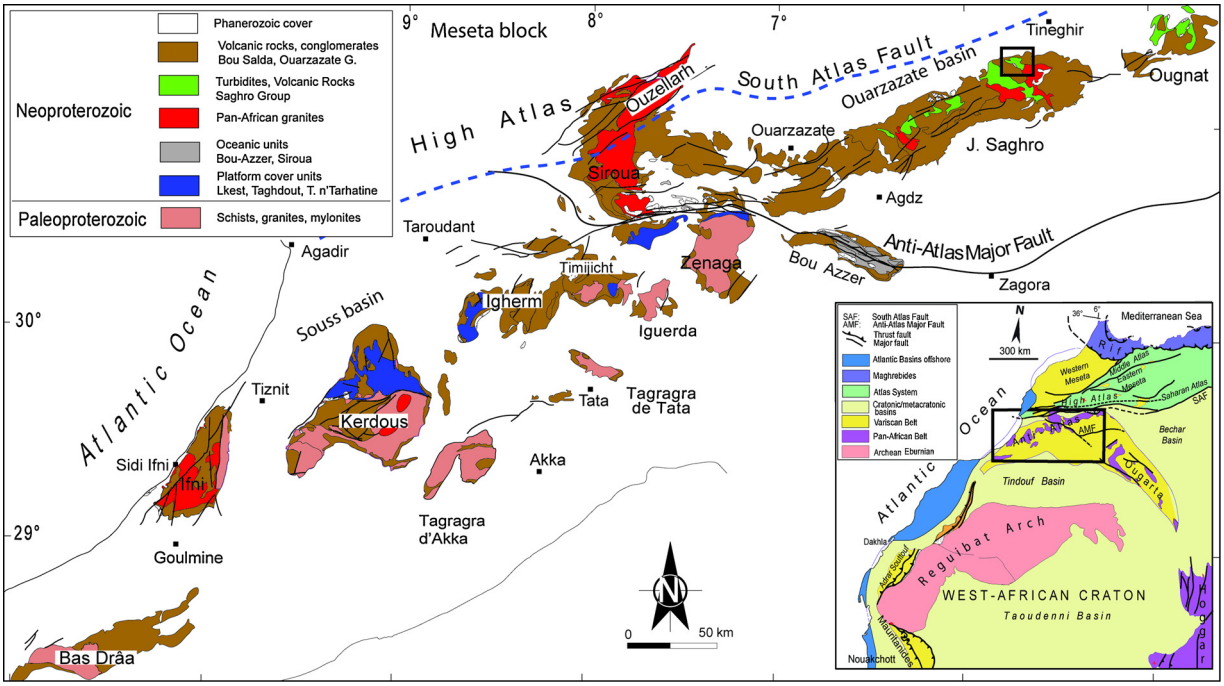

Fig. 2. Geological map of the Anti-Atlas belt in the West African Craton (WAC) showing the location of the studied area (modified from Gasquet et al., 2008).

the northern boundary of the West African Craton, during brittle fracturing of the cratonic boundary.

2.3. Structural setting

The Precambrian inliers of the Anti-Atlas record at least two major orogenic events; a Paleoproterozoic Eburnean event (2–2.1 Ga), and a Neoproterozoic Pan-African orogeny (760 to 550 Ma; Ennih and Liégeois, 2001, 2008; Michard et al., 2008a; El Hadi et al., 2010 and references therein). At the eastern part of the Anti-Atlas, the Saghro massif was affected by successive ductile and brittle deformation events (e.g., Fekkak et al., 2002). Deformation fabrics in the Saghro Massif are associated with three orogenic events, the Neoproterozoic Pan-African orogeny, the Late Paleozoic Variscan shortening, and finally brittle reactivations related to the Atlasic cycle, i.e., Triasic rifting and Cenozoic Africa-Eurasia collision (Michard et al., 2008b).

Along the Bou Azzer-Siroua Neoproterozoic suture, three Pan-African compression phases are descibed; PA1, PA2 and PA3 (Walsh et al., 2012; Hefferan et al., 2014; Blein et al., 2014). PA1 and PA2 correspond to ductile deformations preserved in collages of arc formations in the northern border of the West African Craton. Cryogenian units along the Anti-Atlas major fault suture are deformed by south-

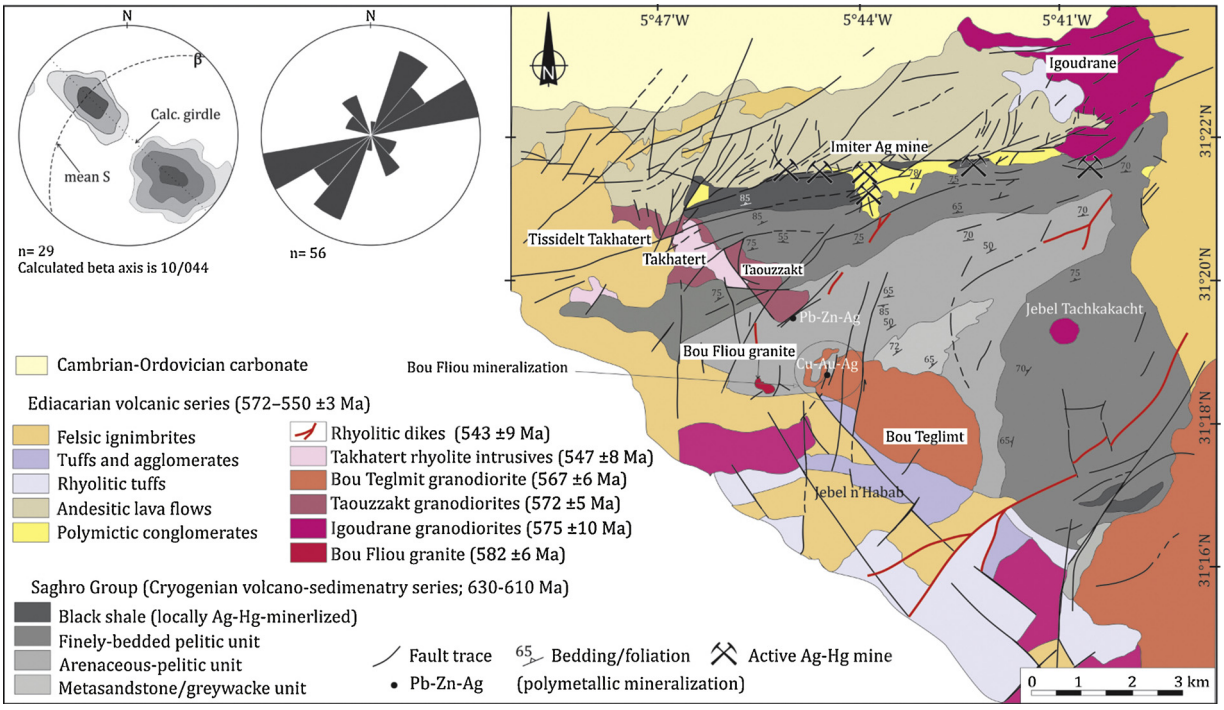

Fig. 3. Geological map of the studied area and directional rosette of the Bou Fliou mineralized structures (n = 22) (modified from Ouguir et al., 1994; Tuduri, 2005).

verging fold and thrust faults of a sinistral transpression regime.

In the Saghro massif, four fault systems are reported (Ouguir et al., 1994; Levresse, 2001; Massironi et al., 2008; Walsh et al., 2012). The NE-SW faults are the most important and are characterized by polycyclic reactivation. Their orientation varies from NE in Boumalne area to ENE in the Imiter domain. This fault system is associated with hydrothermal alteration haloes likely related to volcanic activities in the Saghro area (Ighid et al., 1989; Ouguir et al., 1994; Cheilletz et al., 2002). The polymetallic mineralization in quartz-rich gashes and fault breccias are dominated by hematite, pyrite and chalcopyrite (e.g., Massironi et al., 2008). The E-W faults are common in the Imiter mine area (Ouguir et al., 1994; Cheilletz et al., 2002; Levresse et al., 2004; Tuduri, 2005). These faults are related to the Neoproterozoic transtensional regime and host most of the polymetallic mineralization in the area (Ouguir et al., 1994; Levresse, 2001). N-S to NNW-SSE extensional faults deform the entire area and control the mineralization zones. These faults are associated with polygenic breccias (Ouguir et al., 1994). Some of these faults accommodate a dextral displacement. NW-SE sinistral strike slip faults are extensive and cut all the Precambrian formations at Boumalne area but appear to eliminate in the Palaeozoic cover. Normal fault sets trending in different directions were likely contemporaneous or subsequent to the Late Ediacaran volcanic activities (NP3).

3. Samples and analytical methods

Seventy samples were collected from the principal structure of Bou Fliou mineralization. Forty samples were prepared as polished sections for ore microscopy and textural relationships using the metallographic microscope Olympus BX60. Fifteen samples containing sulphosalt minerals were selected for electron microprobe analysis.

The ore mineralogy, paragenesis and textural features were accomplished by backscattered electron imaging and point analysis. In order to identify areas of interest for microanalysis a SEM at the Reminex Research Center and Laboratory (Marrakech) was used. The chemical compositions of ore minerals (sulphides, sulfosalts and oxides) were determined using a Cameca SX-100 Electron Probe Microanalyzer (EPMA) equipped with five wavelength-dispersive spectrometers, under a 1 μm diameter beam with a voltage of 15 kV, acurrent of 100 nA. and counting time adjusted to 60 s at Service CAMPARIS CNRS-UPMC-IPGP Campus Jussieu (Paris, France). For oxides, analytical conditions are shown in Table 1.

Nine representative samples from the mineralized structures in Bou Fliou mineralization (E1- E9) and one representative sample from Bou Teglimt granodiorite (BT-4) were selected for major and trace element analyses. Approximately 1 g of sample powder was sent to ALS Laboratories in North Vancouver, Canada (http://www.alsglobal.com/) for major, minor and trace element analysis. At ALS, samples were sintered with a lithium metaborate flux before being analysed for 55 major oxide and trace elements by ICP-AES and ICP-MS. The REE and U data are given in Table 4. See the website for further information on analytical conditions and precision.

Table 1
Analytical conditions for microprobe analysis.

Element	Crystal	Line	Sinθa Peak	Background	Counting time (S) Background
Fe	LLIF	Kα	0.48089	0.48089	60
Mg	LTAP	Kα	0.38547	0.38547	60
Al	LTAP	Kα	0.32492	0.32492	60
Si	LTAP	Kα	0.27741	0.27741	60
K	LPET	Kα	0.42759	0.42759	60
Ca	LPET	Kα	0.38391	0.38391	60
Ti	LPET	Kα	0.31425	0.31425	60
V	LLIF	Kα	0.62170	0.62170	60
Cr	LLIF	Kα	0.56869	0.56869	60
Mn	LLIF	Kα	0.52202	0.52202	60
Ni	LIF	Kα	0.41164	0.41164	60
Cu	LIF	Kα	0.38248	0.38248	60
Zn	LIF	Kα	0.35633	0.35633	60

4. Results

4.1. Mineralization characteristics

The Bou Fliou sulfide-magnetite mineralization consists of massive iron oxides and sulfide-rich quartz veins along N- to NE-trending faults cutting the Bou Teglimt granodiorite. The mineralized structures extend for about 1700 m, and their thickness varies from a few cm to > 1 m. Quartz veins are oriented in two distinct directions; N-S and NE-SW. The N-S veins are associated with silicified and chloritized wallrocks, and contain disseminated and blocky masses of sulfides, i.e., arsenopyrite, pyrite and chalcopyrite (Fig. 4). The NE-oriented quartz veins are characterized by sigmoidal geometry and are associated with chlorite and hematite alteration. Besides magnetite and hematite, chalcopyrite, and less abundant pyrite and galena are observed.

Samples collected from the exposure and from the underground levels show disseminated and massive iron oxide and sulfide mineralization, and less dominant breccias and mineralized quartz veins (Figs. 5 and 6). The mineralization in both N-S and NE-SW structures consists mainly of patchy magnetite-hematite domains, replaced in part by chalcopyrite-pyrite-arsenopyrite assemblage, and by a late base metal sulfide assemblage (chlorpyrite-sphalerite-galena, and Bi-sulfosalts; galenobismuthite, lillianite-gustavite, and cosalite). Discrete electrum and free-milling gold particles are observed in some samples, commonly along microfractures in deformed pyrite and arsenopyrite crystals.

Magnetite is the most abundant ore mineral, locally in intergrowth with tabular hematite (Fig. 7). In many samples, magnetite is replaced in part by pyrite and arsenopyrite. Pyrite forms ubiquitous discrete coarse crystals or intergrowths with chalcopyrite and sulfosalts, i.e., cosalite. In some samples, pyrite forms monomineralic veinlets and fills microfractures. Chalcopyrite is ubiqtious in most of the studied samples, where it forms intergrowths with galena, sphalerite and Bi-minerals. In the highly deformed samples, chalcopyrite fills microfractures in magnetite (Fig. 7) or forms dispersed globules intergrown with sphalerite. It also forms patches and fissure fillings in magnetite, and replaces early paragenetic pyrite and arsenopyrite (Fig. 8). Arsenopyrite is less abundant, it forms small grains associated with pyrite or replaced by chaclopyrite. Sphalerite is associated with galena and chalcopyrite (Fig. 9). It is occurring as small inclusions associated with electrum in pyrite crystals. Galena occurs as aggregates of crystals, commonly associated with chalcopyrite and sphalerite (Fig. 9). Cobaltite is less abundant and occurs as subrounded grains embedded in large chalcopyrite patches.

Some Bi-minerals are observed: cosalite ($Pb_2Bi_2S_5$) is commonly associated with chalcopyrite and lillianite-gustavite ($Pb_3Bi_2S_6$ -$PbAgBi_3S_6$) series. It occurs as elongated lamellae or irregular grains in association with chalcopyrite and lillianite-gustavite solid solutions (Fig. 9). In a few samples, Pb-Bi sulfosalts, i.e., galenobismuthite ($PbBi_2S_4$) are observed along fractures in arsenopyrite and chalcopyrite. Gold stringer and specks are commonly dispersed in deformed pyrite. Free-milling gold and electrum grains occur in association with pyrite, chalcopyrite and sphalerite in some samples (Fig. 10).

4.2. EPMA data of sulfide minerals

The electron microprobe (EPMA) data of sulfides disseminated in the mineralized structures are presented in (Table 2). Pyrite contains ≤ 0.57 wt. % Pb and ≤ 0.10 wt. % Zn. The arsenic content varies from 0.09 to 0.36 wt. %. Arsenopyrite has an average arsenic content of 45.52 wt. %. Chalcopyrite shows minor amounts of Pb (≤ 0.15 wt. %)

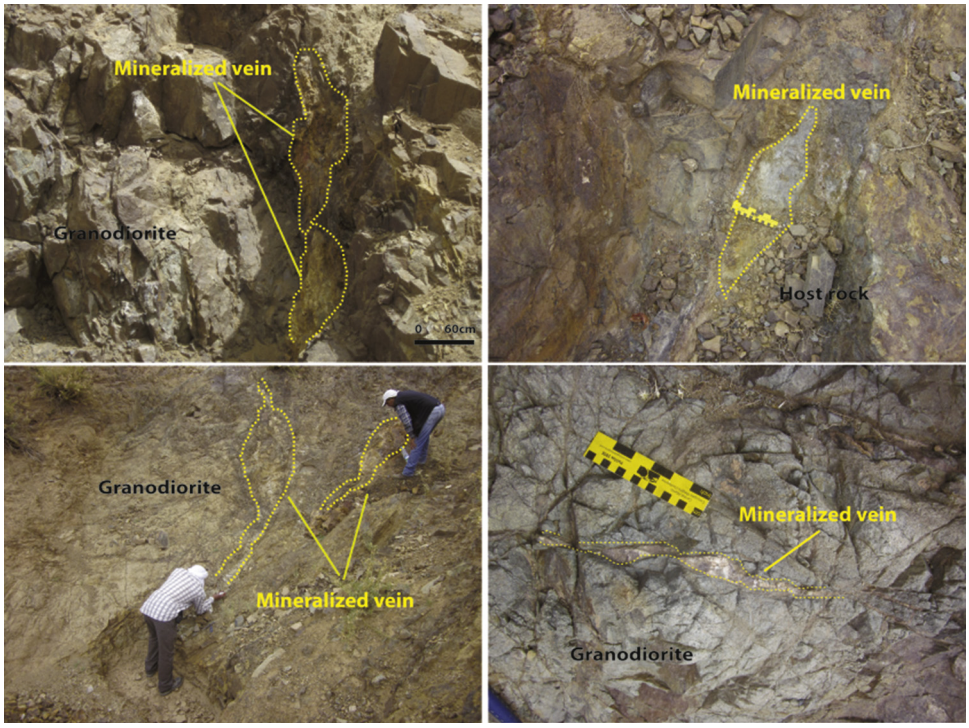

Fig. 4. Mineralized structure with a sigmoidal lense form.

and As (≤ 0.02 wt. %). Whereas, galena contains significant concentrations of silver (≤ 3.11 wt. %), and is therefore considered argentiferous galena.

Bi-Pb sulfosalts (galenobismuthite and cosalite), and Bi-Pb-Ag sulfosalts (lillianite-gustavite series) are identified by ore microscopy and confirmed by the EDS and EPMA data. The EPMA data are given in Table 3, and are plotted on the (Bi + Sb)-(Ag + Cu)-Pb ternary diagram. Galenobismuthite is associated with chalcopyrite along cracks in arsenopyrite. It has minor concentrations of Fe, but very high contents of Bi (61.11 wt %) and Cu (4.72 wt %). Cosalite is deviated from its ideal position in the ternary diagram (Fig. 11), which is likely attributed to the elevated concentrations of Cu (0.32 − 0.93 wt. %) and Ag (1 − 1.36 wt. %) as revealed by EMPA.

Lillianite-gustavite series (Bi-Ag sulfosalts) are reported in NE quartz veins from the Bou Fliou area. These solid solution phases occur as ellipsoidal to irregular crystals and associated with chalcopyrite and

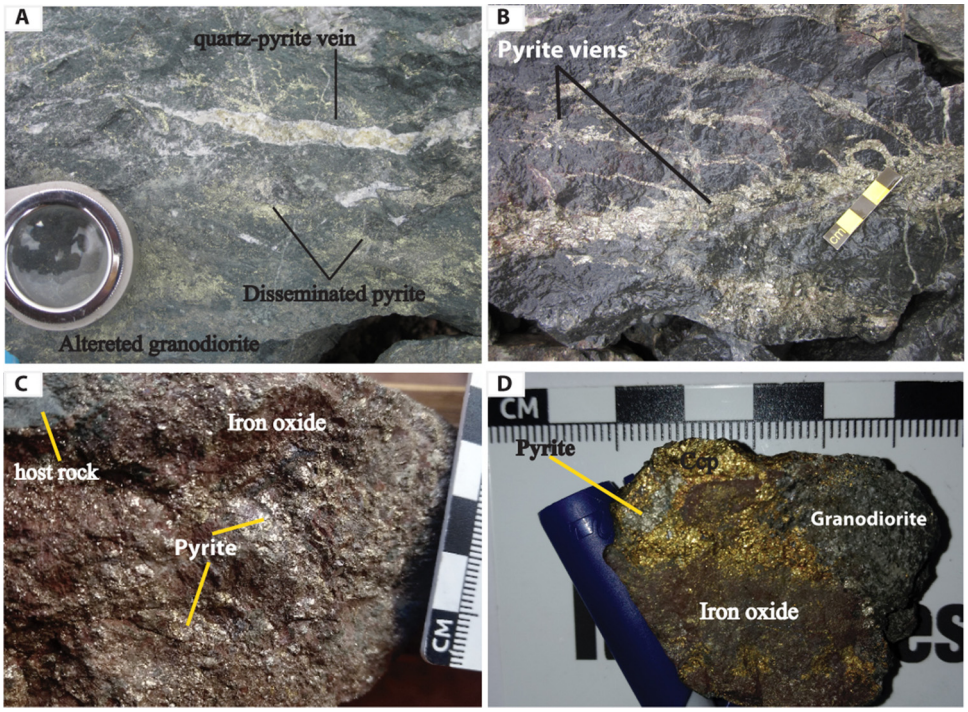

Fig. 5. Macroscopic appearance of Bou Fliou mineralization textures. (A) - Pyrite occurs in veinule associated with quartz (Qtz) and despersed in chloritized facies; (B) - Veinlets filled with pyrite; (C) - Massive pyrite associated with iron oxides (hematite); (D) - Association of chalcopyrite (Ccp), pyrite and hematite.

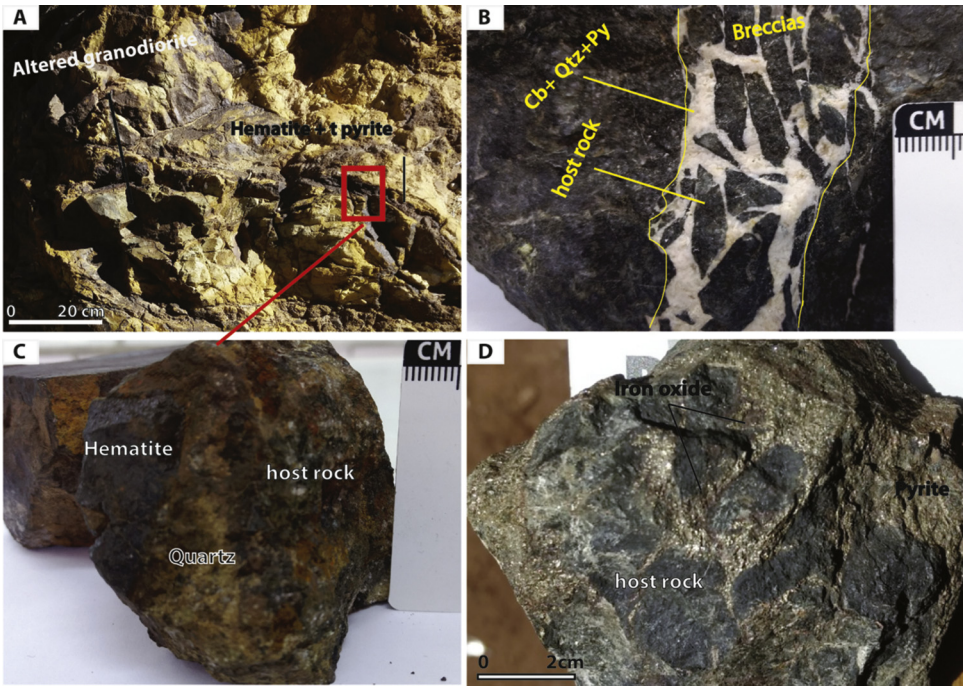

Fig. 6. Macroscopic aspects of Bou Fliou mineralization textures. (A) - Altered granodiorite (casing) intersected by veins of iron oxide (hematite) ;(B) -Sample of the host showing local brecciation essentially filled by a combination of quartz + carbonate + pyrite ;(C) - Sample taken from a vein, filled with hematite + quartz; (D) - Photograph of a breccia zone filled with hematite and pyrite within a chloritized rocks.

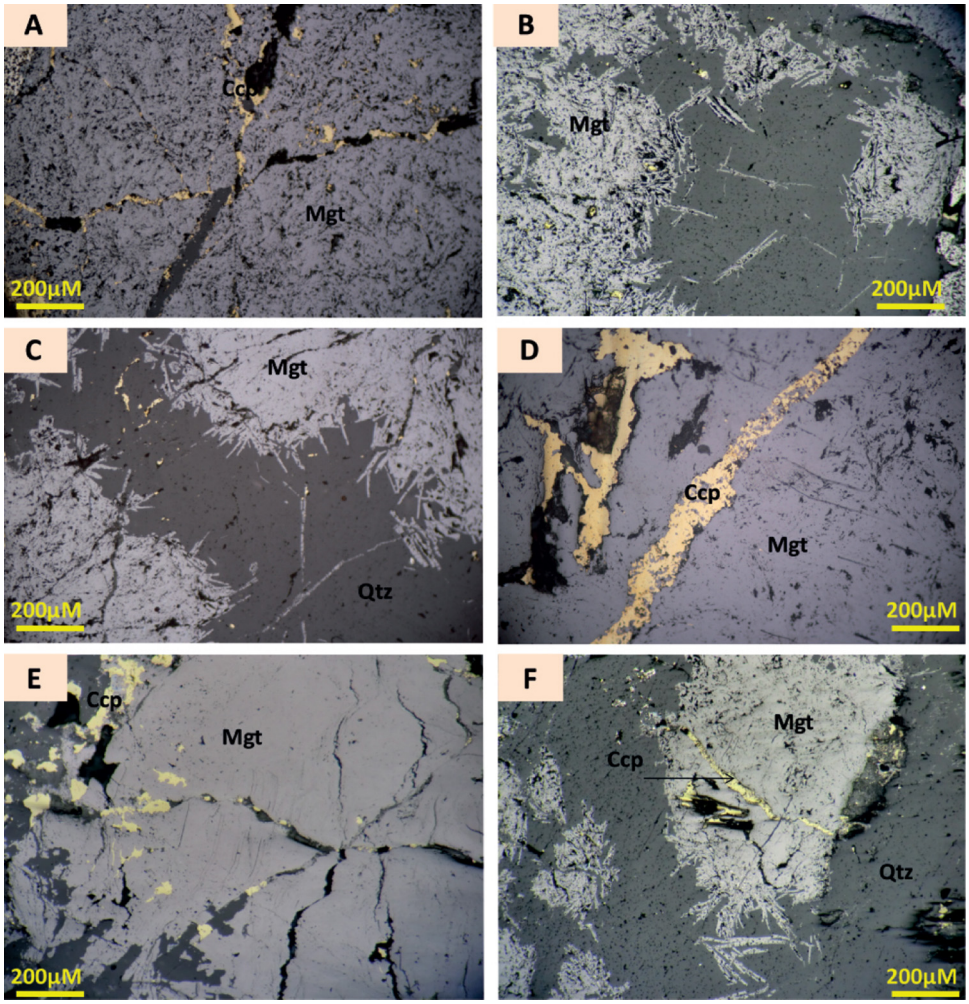

Fig. 7. Microphotographs demonstrating early iron oxide mineralization (reflected light) (A), (B), (F) and (C) - magnetite and flaky hematite with quartz; (D) and (E) - Chalcopyrite filling the fractures have been affected magnetite.

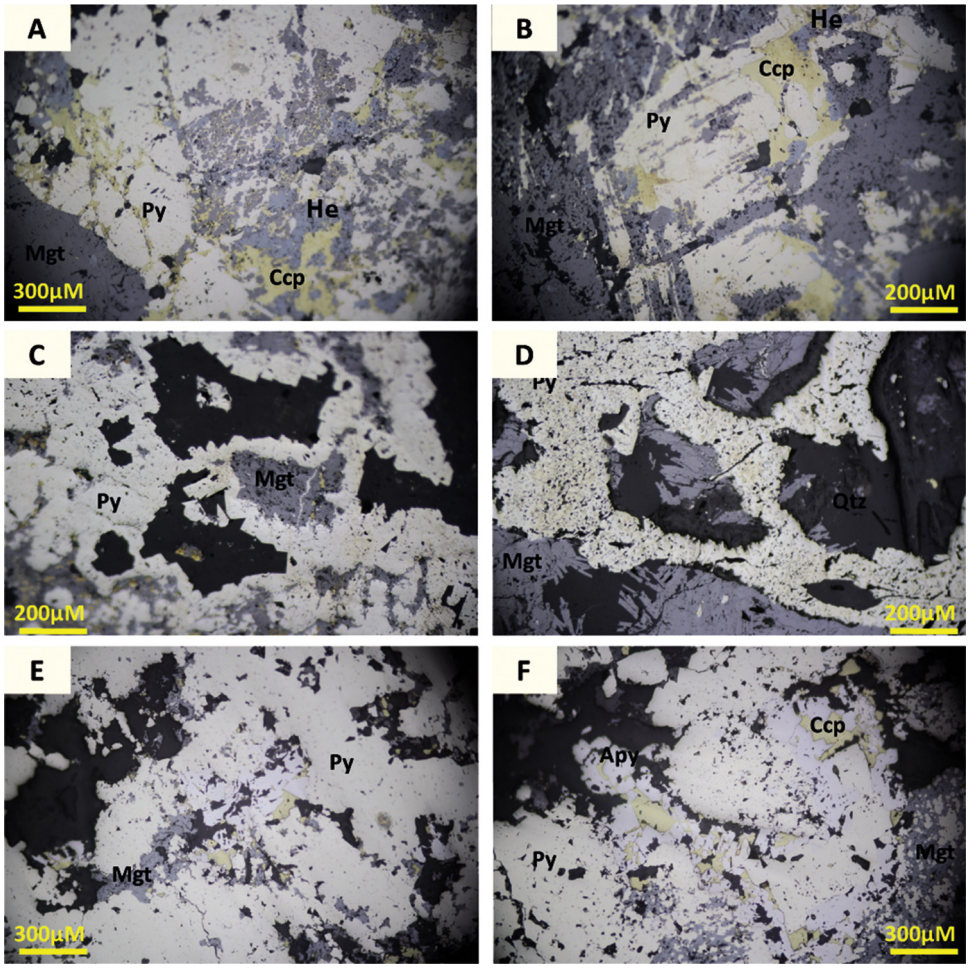

Fig. 8. Microphotographs demonstrating iron oxide replaced by sulphide at Bou Fliou ore deposit (reflected light) (A) and (B)- association of pyrite and chaclopyrite invaded a flake of early magnetite ; (C) and (D) pyrite surrounds magnetite ; (E) and (F) early magnetite overgrow and replaced by association of arsenopyrite, pyrite and chaclopyrite and with late flaky hematite.

cosalite (Fig. 7B). Their chemical data are close to the line of the lillianite-gustavite series on the (Bi + Sb) − (Ag + Cu) –Pb diagram (Fig. 11).

4.3. EMPA data of iron oxides

The electron microprobe (EPMA) data of iron oxides are given in Table 4. The analyzed elements are plotted in a decreasing order of abundance on the multi-element spider diagram. The iron oxides from the Bou Fliou mineralization show roughly a uniform pattern (Fig. 12B). According to Beaudoin and Dupuis (2007; 2011), the spectrum of the investigated iron oxides corresponds to the IOCG (Fig. 12A). It generally has average concentrations of all elements, but a slight depletion in K and mild depletions in Cr, Ti and V. On the Ca vs Ti + V discriminating diagram (Beaudoin and Dupuis, 2007; Dupuis and Beaudoin, 2011), most data points of the analyzed iron oxides plot in the IOCG field (Fig. 13).

4.4. Paragenetic sequence

The ore microscopy studies indicate three overprinting events in the Bou Fliou mineralization, namely: (I) an early iron oxide mineralization, (II) a partial Fe-As sulfide replacement event, and (III) late-genetic base metal replacements, stockworks Pb ± Ag ± Bi- sulfosalts and gold, and quartz and calcite-rich veins (Fig. 14). Other, mostly supergene, late hydrothermal minerals include malachite and azurite.

4.4.1. The early iron oxide mineralization

Magnetite constitutes the main ore mineral, forming monomineralic patchy masses or intergrowths with hematite and goethite. The abundant magnetite in the fractured granodiorite host rocks makes the ore zones easily recognizable as black colored zones along fracture/joint systems. Locally, magnetite crystals are fractured or brecciated and cut by veins of apatite–quartz or calcite–-chlorite–quartz–pyrite–chalcopyrite associations. The blocky magnetite bodies are cut by narrow zones of potassic alteration (K-feldspar–biotite–magnetite–quartz), which forms the locus for the Cu–Au mineralization. Hematite could be the result of martitization of early magnetite or a supergene oxidation phase. It occurs commonly as acicular laths or as bands interlayered with magnetite. Quartz and calcite commonly occur in zones characterized by magnetite replacement by hematite.

4.4.2. The Fe-As sulfide replacements

This mineralization type is most abundant in the brecciated rocks, where massive pyrite and arsenopyrite, and associated stockwork veins cut the magnetite-rich zones. Cobaltite is a less abundant phase, commonly as fine disseminations near the margins of large magnetite patches. Microscopic textures include replacement along crystallographic planes of magnetite, remnant islands of the nonreplaced magnetite and/or hematite, rims of sulfides surrounding large aggreagates of magnetite-hematite, and fractures in magnetite healed with pyrite and arsenopyrite intergrowths. Idiomorphic pyrite and arsenopyrite crystals

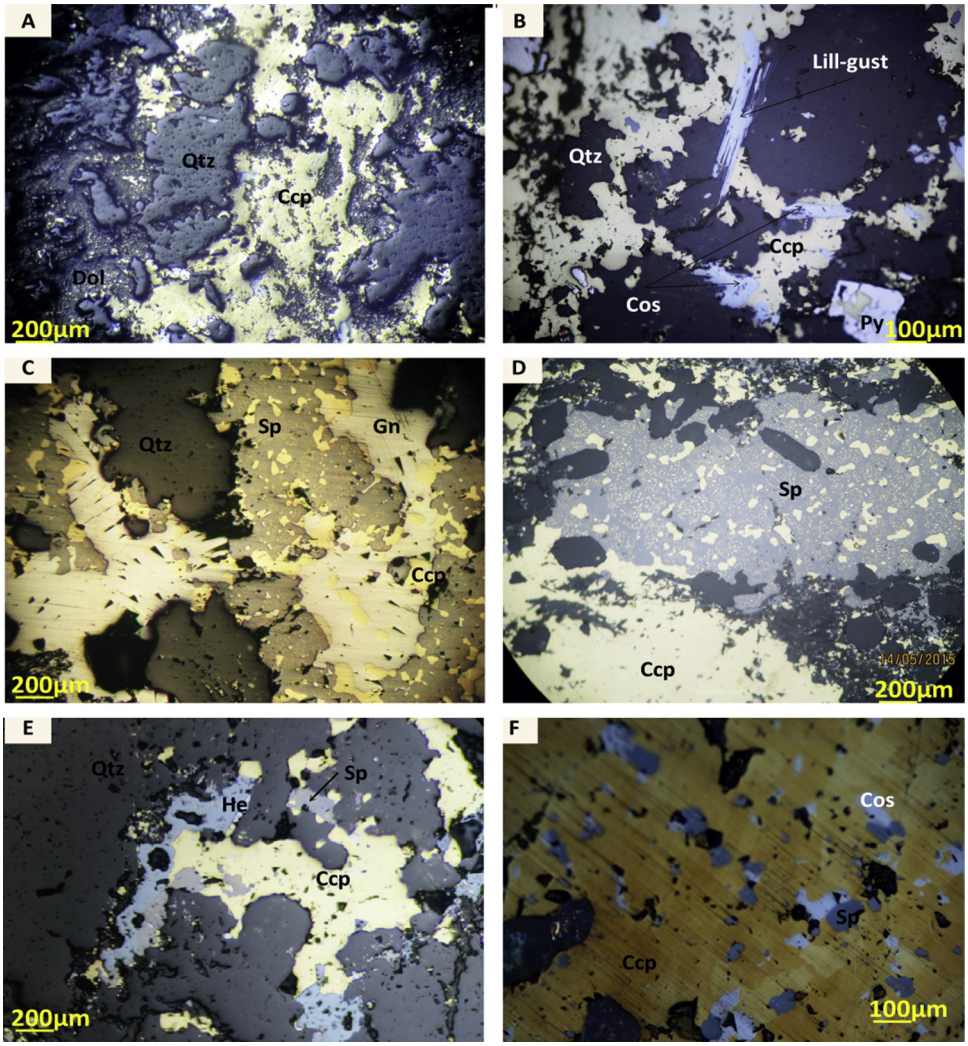

Fig. 9. Microphotographs demonstrating sulphide and sulphosalt paragenesis at Bou Fliou ore deposit (reflected light) (A) Quartz remains surrounding by chalcopyrite and dolomite; (B) blue laths of Lillianite-gustavite (lill-gust) seriein close association with, cosalite (Cos) and chalcopyrite (C) Association of chalcopyrite, galena and sphalerite; (D) sphalerite with « chalcopyrite disease ». (For interpretation of the references to colour in this figure legend, the reader is referred to the web version of this article).

occur commonly at the center of the large patchy masses, where they are also replaced by a later Cu-Zn sulfide mineralization.

4.4.3. Base metal replacements, stockworks Pb ± Ag ± Bi- sulfosalts and gold

This is a late polymetallic mineralization stage, characterized by abundant Cu-Zn-Pb sulfides, in addition to less common pyrite. Chalcopyrite, sphalerite, galena and minor amounts of galenobismuthite and sulfosalts replace the early paragenetic pyrite and arsenopyrite and iron oxides. Chalcopyrite heals fractures with or without sphalerite. Pyrite forms monomineralic veinlets in the pyrite-arsenopyrite domains. Bi- minerals are represented mainly by the galenobismuthite. The chalcopyrite-galenobismuthite assemblage fills microcracks in the early arsenopyrite. Cosalite and lillianite-gustavite occur generally as dispersed flakes and tabular crystals, commonly in association with chalcopyrite. Scarce fine particles of free-gold and electrum occur as secondary fillings in fractured pyrite. The gangue minerals associated with this stage of mineralization include quartz, dolomite and chlorite.

4.5. Hydrothermal alteration and structural controls

Hydrothermal alteration is commonly recognized along and next to the mineralized structures. The common alteration types include: widespread muscovite and local chlorite and carbonate alteration. A late K-feldspar overprint and hematitic alteration are confined to the mineralized fault intersections. These alteration phases form vein networks that impose all early alteration types.

Widespread secondary K-feldspar is disseminated in the bleached host rocks or represented by millimeter to centimeter thick veinlets cutting the host granodiorite rocks (Fig. 16A, B). Biotite in the host granodiorite is partially or completely replaced by musco. Hydrothermal silica and quartz veins, stockworks are commonly reported in association with potassic alteration in the mineralized zones (Fig. 16E). Fragments of the Bou Teglimt granodiorite are cemented by a silica-rich matrix (Fig. 16F). The quartz-hematite-K-feldspar-rich zones may contain small dispersed uranirite grains, reported during the SEM studies.

Chlorite, and dolomite and less common calcite are common along the mineralized structures (Fig. 17C and D). Chlorite and epidote progressively replace granodiorite to the point where it becomes very penetrative and completely texture-destructive (Fig. 15 C and D) (Fig. 16 C). It occurs especially proximal to the mineralized zones. Epidote is developed at the expense of amphibole, where it appears as centimeter-wide veinlets cutting the host granodiorite. The mineralized structures are locally associated with zones of intense scapolite alteration (e.g., Moreto et al., 2014). In the Bou Fliou site, magnetite and hematite are

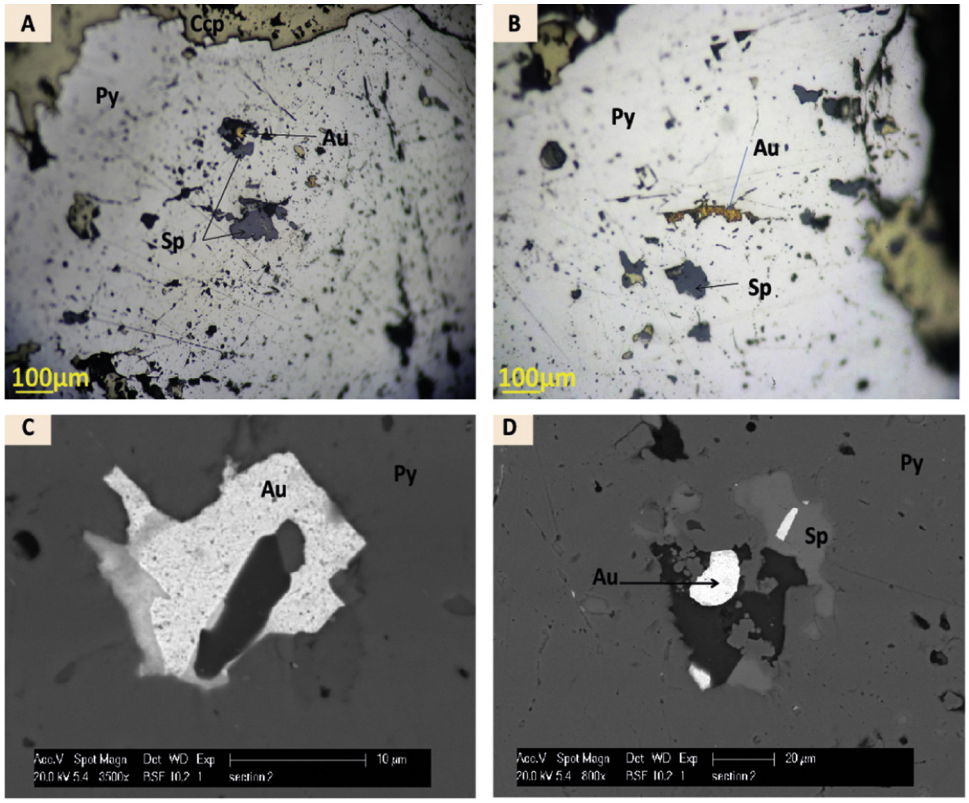

Fig. 10. Microphotographs (reflected light) and SEM photomicrographs of gold (A)-electrum (Au-Ag) in close association with sphalerite (Sp) inclusions within pyrite; (B)- electrum (Au-Ag) inclusions in pyrite;(C) and (D): Inclusions of electrum (Au-Ag) in pyrite.

mainly associated with quartz, chlorite ± dolomite.

Carbonate alteration is commonly associated with disseminations of chalcopyrite (Fig. 17D), or forms veinlets cutting the host rock and mineralization (Fig. 15C and E). Dolomite is the most abundant and yields atomic compositions of Ca (5.25%), Fe (0.33%) and Mg (7.98%), while the late carbonate veins are mainly made up of calcite.

The mineralized N-S faults are either extensional faults or accommodate a slight dextral offset. The NE-SW faults are sinistral strike slip faults intersecting and displacing the older N-S faults and related veins (Fig. 18). It is hard to interpret these faults as conjugate sets of a NW-SE compressional regime. Field observations suggest that the Imiter fault network was developed by an extensive transcurrent deformation event during the Late Neoproterozoic and likely controlled the scattered mineralization (e.g., Ouguir et al., 1994, 1996; Levresse, 2001; Tuduri, 2005). The NE-SW mineralized structures at the Bou Fliou area can be attributed to the B regime defined by Ouguir et al. (1994) and Levresse (2001). The N-S mineralized structures can be linked to the sub-meridian (N-S to NNW-SSE) fault family described by Ouguir et al. (1994).

Table 3
Representative EPMA data of Bi-sulfosalts in the Bou Fliou ore deposit.

	Cosalite					Lillianite-gustavite serie	Galenobismuthite
Wt%							
S	14.85	15.24	14.94	15.18	14.57	14.99	16.63
Fe	0.28	–	0.13	0.08	–	1.42	1.00
Co	–	–	–	0.02	–	0.02	–
Ni	–	0.02	–	–	0.02	0.01	0.04
Cu	1.39	2.59	1.29	1.33	1.02	1.83	4.73
Zn	–	–	0.01	0.03	–	0.04	–
Sb	1, 28	0.88	0.91	0.88	1.44	0.17	0.19
As	–	–	–	–	–	–	0.03
Se	0.10	0.09	–	–	–	0.03	0.07
Ag	1.37	1.00	1.35	1.32	1.15	4.50	–
Pb	37.10	37.15	37.51	37.59	37.10	33.83	15.81
Bi	42.66	42.33	43.75	43.11	41.62	43.30	61.12

Table 2
Representative EPMA data of sulfide minerals from the Bou Fliou ore deposit.

	Chalcopyrite		Arsenopyrite	Pyrite					Cobaltite
Wt%									
S	33.04	33.38	18.63	51.95	51.75	51.68	51.73	51.58	19.61
Fe	30.00	29.45	34.64	45.78	45.35	44.72	44.93	45.56	1.60
Co	–	–	–	–	–	–	–	–	32.71
Ni	–	0.02	–	–	–	–	0.02	0.01	0.55
Cu	34.07	33.99	0.09	0.10	0.02	–	–	0.08	0.07
Zn	0.02	0.02	0.04	–	–	–	–	0.03	–
As	0.02	–	45.52	0.09	0.19	0.33	0.16	0.36	43.10
Ag	–	–	–	–	–	0.02	–	–	–
Pb	0.04	0.16	0.01	0.41	0.20	0.15	0.46	0.57	0.17
Bi	–	–	–	–	–	–	–	–	–

Table 4
Chemical composition of iron oxides (magnetite and hematite) from the Bou Fliou ore deposit.

Iron Oxides (wt%) Magnetite/Hematite	Si	Al	Mn	Mg	Ti	V	Zn	Cr	Cu	Ni	Ca	K
1	0.287	0.031	0.014	0.045	0.005	0.002	–	–	–	0.008	0.036	0.026
2	0.864	0.094	0.017	0.038	0.009	0.009	0.008	0.001	–	0.012	0.110	0.050
3	0.927	0.067	0.019	0.041	0.009	–	–	0.001	0.005	–	0.059	0.012
4	0.340	0.316	0.023	0.080	0.003	0.005	0.006	0.003	0.040	–	0.069	0.032
5	0.800	0.083	0.015	0.041	0.007	0.004	–	0.003	–	–	0.067	0.033
6	1.213	0.176	0.019	0.062	0.020	0.005	0.009	0.003	0.012	0.005	0.129	0.089
7	0.280	0.017	0.012	0.046	0.009	0.008	–	–	–	–	0.028	0.109
8	1.425	0.122	0.015	0.044	0.025	0.010	0.013	0.001	0.043	0.003	0.142	0.055
9	1.579	0.150	0.022	0.042	0.018	0.006	0.025	–	0.008	0.008	0.147	0.061
10	0.200	0.018	0.014	0.044	0.005	0.010	0.032	0.002	–	0.018	0.032	0.029
11	1.665	0.094	0.023	0.042	0.010	0.002	0.042	–	–	–	0.095	0.020
12	1.092	0.152	0.020	0.064	0.018	0.008	–	–	0.098	0.006	0.246	0.096
13	0.958	0.204	0.036	0.077	0.011	0.012	–	0.002	0.008	0.010	0.075	0.016
14	0.450	0.024	0.013	0.036	0.006	0.009	0.017	–	–	–	0.023	0.014
15	0.109	0.014	0.016	0.038	0.008	0.009	0.009	0.001	0.011	0.010	0.013	0.017
16	0.662	0.094	0.024	0.054	0.006	0.003	–	0.002	0.007	0.014	0.027	0.014
17	1.801	0.173	0.030	0.033	0.009	0.001	0.037	0.003	–	0.006	0.104	0.022
18	0.105	0.012	0.010	0.036	0.001	0.008	–	–	0.020	0.014	0.007	0.022
19	1.095	0.121	0.016	0.033	0.010	0.004	–	0.002	–	0.014	0.076	0.067
20	0.115	0.020	0.021	0.033	0.004	0.003	0.015	–	0.002	–	0.010	0.012
21	0.553	0.094	0.038	0.040	0.002	0.001	–	0.002	–	0.006	0.053	0.031
22	0.165	0.018	0.017	0.042	0.003	0.003	0.001	–	–	0.009	0.015	0.013
23	0.425	0.274	0.052	0.098	0.002	0.006	–	–	0.002	0.018	0.021	0.011
24	1.179	0.104	0.016	0.042	0.012	0.005	–	–	–	0.003	0.071	0.025
25	0.107	0.125	0.022	0.043	0.002	0.001	–	0.003	–	0.022	0.033	0.016
26	0.070	0.017	0.013	0.039	0.001	0.008	–	–	–	–	0.015	0.013
27	0.175	0.183	0.021	0.164	0.006	0.004	0.003	–	0.014	–	0.012	0.043
28	1.052	1.138	0.075	0.355	0.005	0.005	0.022	0.001	0.029	0.014	0.030	0.034

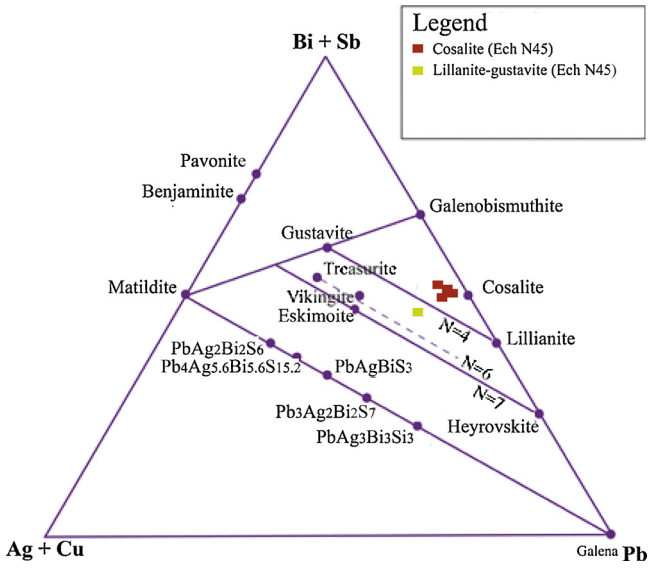

Fig. 11. Ternary diagram of Bi-Pb and Bi-Pb-Ag sulfosalts from the Bou Fliou mineralization.

5. Discussion

The evolution of the Imiter inlier involved polyphase magmatism and crustal scale faulting. The Bou Fliou mineralization is hosted in strucutres deforming the Bou Teglimt granodiorite (567 ± 6Ma). Recent geochronological and geochemical studies done on the Imiter granitoids identify two types of granitoids (e.g., Baidada et al., 2018 In press): i) calc-alkaline granitoids (the Bou Teglimt granodiorite, Taouzzakt, Bou Fliou granite) formed in a continental arc environment, and ii) high-K calc-alkaline granitoids (Igoudrane quartz-diorite) marks the final stage of Pan-African orogeny in a post-collisional setting related to either modification of the margin of the West African Craton or to formation of a continental volcanic arc above a short-lived south-dipping subduction zone (Walsh et al., 2012; Baidada et al., 2018).

The extensive magmatic activity at the end of the Ediacaran, was likely associated with hydrothermal systems, responsible for the formation of several base metal deposits in the Eastern Anti Atlas and in the Imiter inlier in particular (e.g., Levresse, 2001; Abia et al., 2003; Gasquet et al., 2005; Tuduri, 2005). The most important are the Bou Madine epithermal deposit at (Pb-Zn-Cu-Ag-Au) in the Ougnat inlier, the Imiter (Ag-Hg) epithermal deposit (Tuduri, 2005; Levresse, 2001), and the Tiouit (Au-Cu-Ag) porphyry deposit (Alansari, 1997; Bouabdellah et al., 2016) in Boumalne inlier (Table 6).

The Bou Fliou occurrence is a polymetallic Cu-Au-Ag mineralization hosted by NE and N-S faults that could be considered high-order splays or reactivation structures of the main Late Neoproterozoic, ENE-WSW transcrustal Imiter fault. Tectonic reactivation and thermal events are ascribed to post-kinematic intrusions (e.g., 547 ± 26 Ma; Thomas et al., 2004) and later until during the Hercynian orogeny (Levresse et al., 2016 and references therein). Successive and overpriniting silver mineralization events in the giant Imiter Hg-Ag deposit are related to contact metamorphism of Cryogenian carbonaceous schsits by the ca. 572 Ma calc-alckaline granodiorite intrusions, while significant epithermal silver mineralization formed conceurrent with the intrusion of post-kinematic intrusions (~550 Ma, Cheilletz et al., 2002; Levresse et al., 2004). Later remobilization of Ag–Hg minerals took place at ~255 Ma (Borisenko et al., 2013).

The paragenetic sequence of the Bou Fliou mineralization comprises three successive mineralization stages, namely: (I) an early iron oxides stage, (II) an intermediate arseno-ferriferous stage (As-Fe), and (III) a polymetallic stage with Cu-Zn-Pb-Au-Ag associated with a gangue composed mainly of quartz-dolomite. The third stage corresponds perfectly to the main mineralization stage in the paragenesis of the Imiter (Ag-Hg) and Tiouit (Au-Cu-Ag) deposits (Vargas, 1983; Guillou et al., 1988; Ouguir et al., 1994; Baroudi et al., 1999; Levresse, 2001; Tuduri, 2005; Gasquet et al., 2005). The EPMA data of the magnetite-hematite assemblage show low levels of Ti. The presence of Bi-sulfosalts could be had a significant effect to act as gold scavenger (Ciobanu et al.,

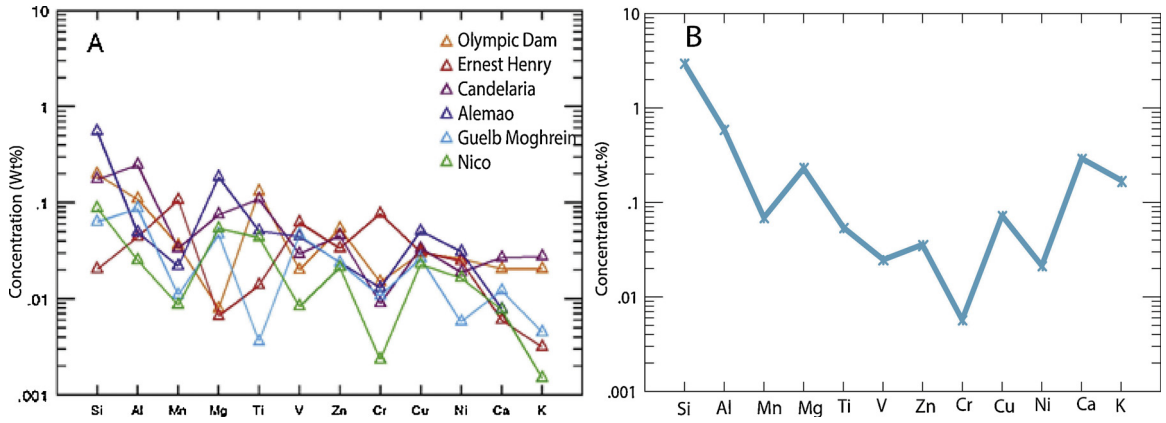

Fig. 12. A) Diagram showing chemical composition of iron oxides from IOCG ore deposits (Beaudoin and Dupuis,2007); (B) Chemical composition of iron oxide minerals from the Bou Fliou mineralization.

2006; Ilmen et al., 2015)

According to Barton et al. (2005), the IOCG deposits tend to form at 4–6 km from low CO_2 high-salinity (10–35 wt % $NaCl_{eq}$) fluids, similar to porphyries, and are variably associated with crustal-scale structures. Many of them are characterized hydrothermal alteration zoning, in which a relatively oxidized, commonly more sulfide- and K-rich assemblages at high levels to relatively reduced (magnetite-rich), sulfide-poor assemblages with extensive Na-(calcic) alteration at depth (e.g., Hitzman et al., 1992; Barton and Johnson, 2000). Intrusion-induced heating of mixing surface and deep sourced fluids will lead to over-pressured fluids (steam), that fracture the host rock and form breccias with high iron content (e.g., Williams, 2010).

The quartz diorite of Igoudrane (and Takhatert rhyolite) represents the youngest magmatic activity (538 ± 6 Ma) in the Imiter inilier (Baidada et al., 2018). Emplacment of this high-K calc-alkaline intrusion was likely accompanied by the development of a fault system in the pre-existing arc calc-alkaline rocks (e.g., Ouguir et al., 1994; Levresse, 2001) (Fig. 19). The inteplay of intrusion-induced heating and mixing of shallow and deep fluids promoted extensive hydrothermal alteration, local enrichment in light REE and Au (Table 5 and Fig. 20), and deposited scattered Fe-Cu and Au-base metal mineralization under oxidizing conditions, typically described for IOCG deposits (Table 7). This should motivate new exploration programs for more world-class or

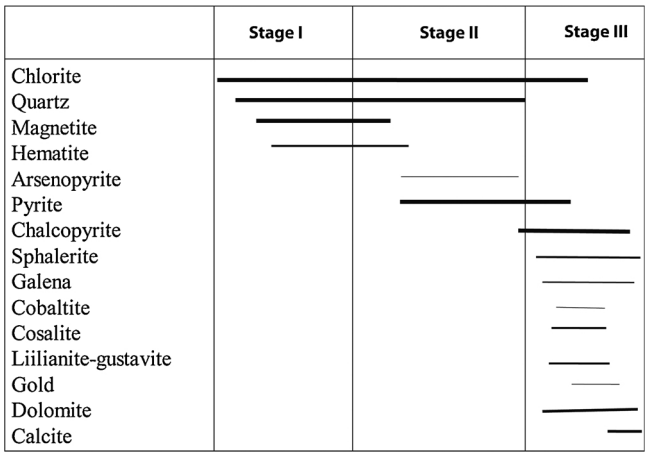

Fig. 14. Paragenetic sequence for the Bou Fliou mineralization.

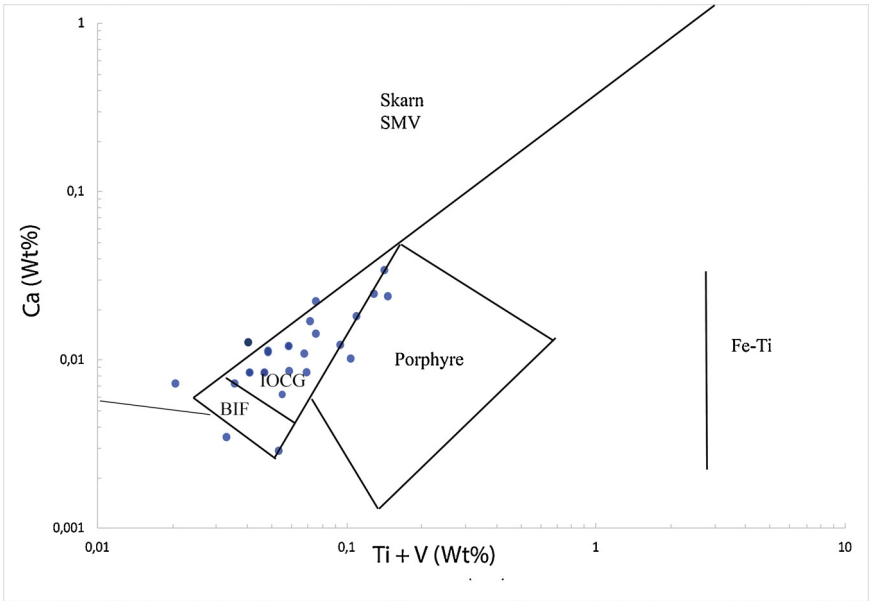

Fig. 13. Ca vs. Ti + V discriminate diagram showing the position Bou Fliou iron-copper mineralization (Beaudoin and Dupuis, 2007).

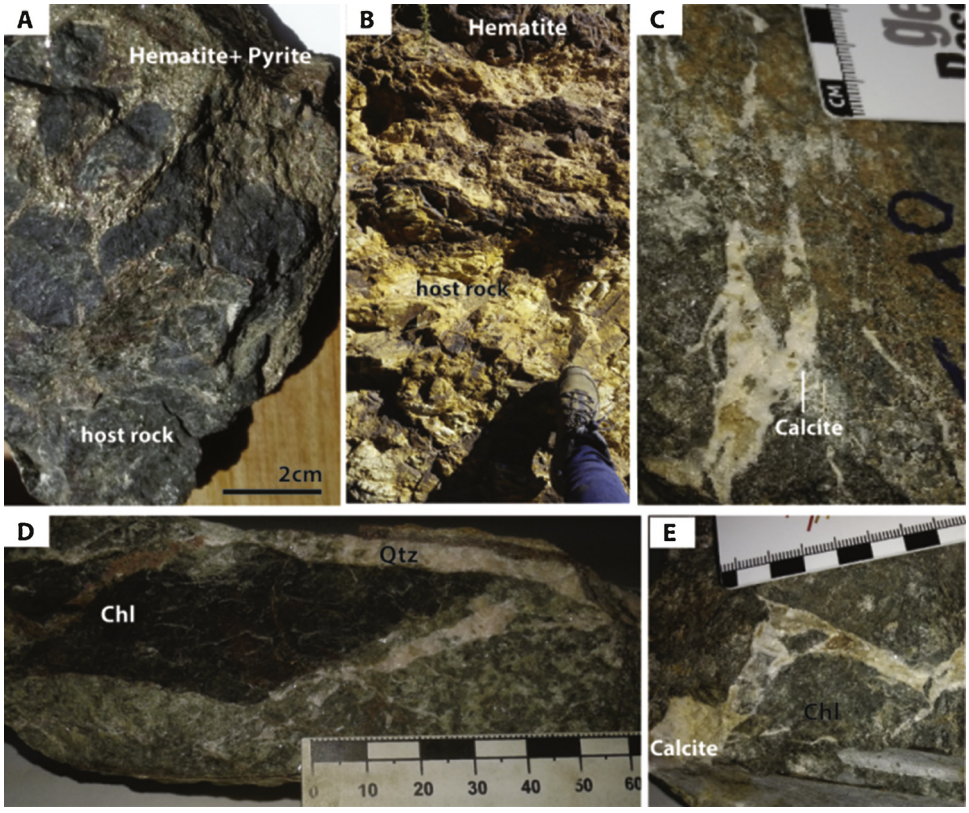

Fig. 15. Photographs of Bou Fliou hydrothermal alteration aspects. (A) - Hematite + pyrite breccia ; (B) - Hematite veins affect the Bou Teglimt granodiorite ; (C) and E) - calcite veins ;(D) - Band of chlorite bounded by two veinlets of quartz in a granodioritic facies.

giant deposits in the Imiter inlier region.

6. Conclusion

This work describes new data from the polymetallic Cu-Au-Ag mineralization hosted by the Bou Teglimt granodiorite. Key trace minerals (iron oxides, Bi-sulfosalts, base metals), field observations, geochemical, hydrothermal and structural features are discussed demonstrating their genetic significance in relationship to ore formation of the Bou Fliou deposit. With regards to close association of iron oxides and

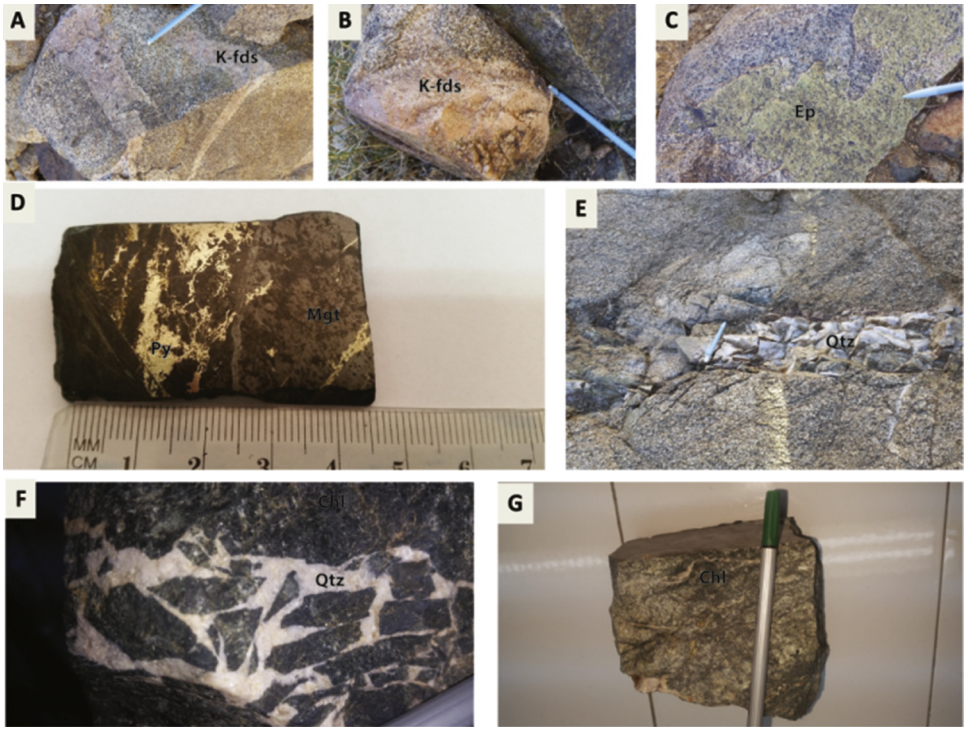

Fig. 16. Photographs of selected features of the hydrothermal alterations from the Bou Fliou ore deposit. A) and B) Pink K-feldspar veins cutting the Bou Teglimt granodiorite; C) Epidote rich-fractures cutting the granodiorite ; D) Polished sections showing association of magnetite, pyrite and chlcopyritee ; E) centimeter-sized-quartz veins cutting the granodiorite; F) Photograph showing hydraulic breccias with chloritized fragments of granodiorite cimented by quartz G) Chlorite bearing veinlets cutting the granodiorite.

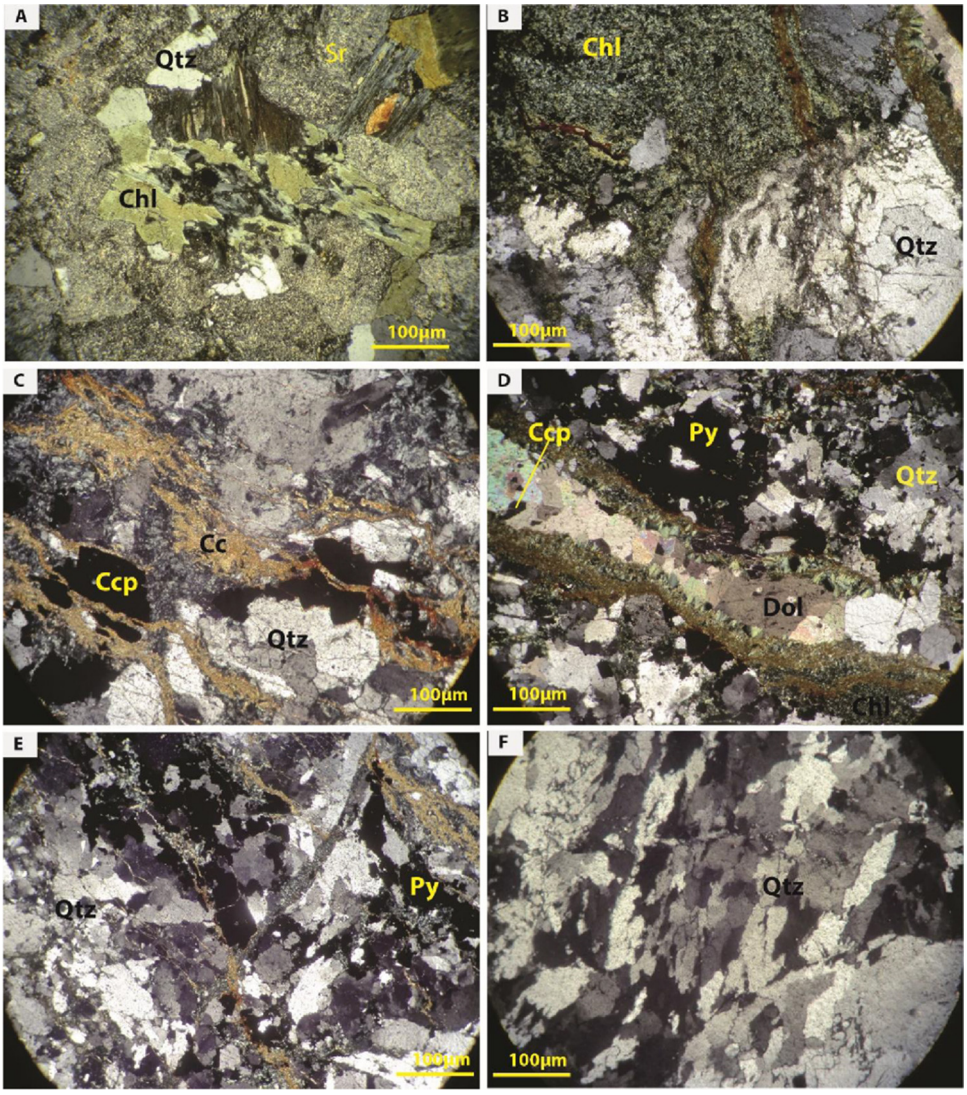

Fig. 17. Microphotographs of the selected hydrothermal alteration observed in transmitted light (A) - Chloritised biotite with partially to totally serticized plagioclases; B) - Penetrative alteration with development of chlorite masses; C) - Late microfissures filled by calcite associated with chalcopyrite; (D) - The carbonate veinlet rims are chlorite enriched rims; (F)- Elongated quartz crystals (mylontic texture); (E)- Vein of quartz associated with pyrite.

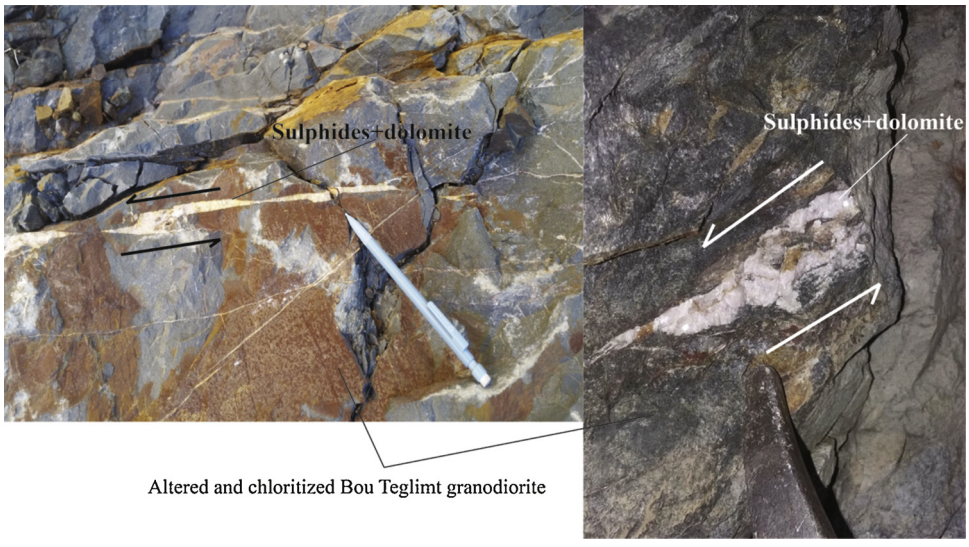

Fig. 18. Field photographs showing sinistral carbonate (dolomite) veins cutting the Bou Teglimt granodiorite.

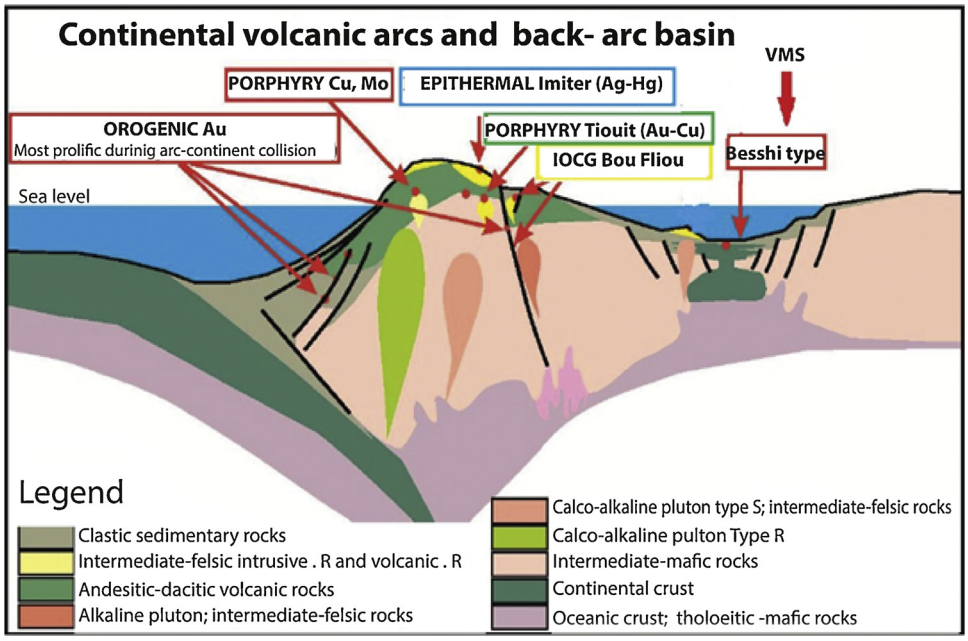

Fig. 19. Schematic illustration showing the position of different types of the Saghro ore deposits in an ocean-continent subduction context. The polymetallic iron oxide (IOCG) deposits are located along crustal faults in association with alkaline felsic intermediate plutonism. In the same tectonic environment, IOCG is associated with Cu-Au porphyry and epithermal deposits. The model is modified from (Lydon, 2007 and Benoit, 2000).

Table 5
Representative REE, Au and U data (in ppm) of the Bou Fliou mineralization and host granodiorite rocks.

Samples	La (ppm)	Ce (ppm)	Pr (ppm)	Sm (ppm)	Eu (ppm)	Nd (ppm)	Gd (ppm)	Tb (ppm)	Dy (ppm)	Ho (ppm)	Er (ppm)	Tm (ppm)	Yb (ppm)	Lu (ppm)	U (ppm)	Au (ppm)
BT- 4	18	34	3.9	3.1	0.9	16	2.9	0.4	2.7	0.6	1.5	0.2	1.4	0.2	1.82	–
E1	29.1	63.3	7.16	6.61	1.34	28.6	5.3	0.72	4.06	0.79	2.08	0.31	1.8	0.3	2.22	0.18
E2	35.3	71	7.96	7.3	1.34	32.3	6.02	0.86	4.6	0.89	2.33	0.33	1.86	0.28	1.63	4.26
E3	18.8	35.1	4.18	3.74	0.74	16.6	3.41	0.48	2.68	0.56	1.44	0.24	1.25	0.21	1.18	2.39
E4	44	78.9	9.52	8.87	1.42	38.5	6.89	0.99	5.6	1.12	2.94	0.45	2.72	0.41	2.07	3.24
E5	33.8	59.6	7.38	7.19	1.13	29.8	6.1	0.87	5.45	1.1	2.9	0.49	2.74	0.44	1.98	1.02
E6	12.4	22.7	2.73	2.92	0.75	10.9	2.48	0.4	2.39	0.49	1.19	0.18	1.18	0.18	0.96	0.52
E7	20.8	39.3	4.72	4.59	1.63	19.2	4.24	0.6	3.46	0.66	1.84	0.28	1.71	0.27	1.19	0.2
E8	25.8	49.2	6.01	5.62	1.67	23.8	5.04	0.68	4.03	0.79	2.09	0.32	1.83	0.29	1.53	0.24
E9	19	37	4.48	3.87	1.12	18	3.51	0.5	2.88	0.58	1.57	0.25	1.49	0.25	2.01	–

Table 6
Synthesis on the different deposits listed in the Eastern Anti Atlas.

Deposit	Host rock	Ore bodies and structures	Hydrothermal alteration	paragenesis	References
Bou Madine	Volcanic rock (ignimbrite and andesite)	Quartz veins along N 160° (N-S) faults	Quartz-sericite-chlorite-calcite	Two paragenetic stages Stage Fe-As : Py + Sp + Aspy + Pyro PolymetallicStage : Sp + Ccp + Gal + Ag- minerals and Bi-minerals	Levresse, 2001 Abia et al., 2003 Paile, 1983
Tiouit	Tiouit Granodiorite	Quartz veins along N 10°	Biotite-sericite-quartz Chlorite-quartz-calcite Hematite	Four paragenetic stages Stage Fe-As : Mgt + Py + Aspy PolymetallicStage : Ccp + Gal + AspII + Bi + Te + Sb Hematite + Au Satge Oxydation-cimentation	Alansari, 1997 Bouabdellah et al., 2016
Imiter	Black shales	Disseminated ore and mineralized quartz veins along N 60° E-W faults	Quartz-calcite Quartz-chlorite-muscovite Quartz-dolomite	Four paragenetic stages Stage : Py Stade : Pb + Zn + Cu + As Polymetallic Stage : Qtz + Pb + Ag+Hg + Py + Gal + Sp + Ccp Dol + Ccp + Py + Gal + Ag + Sp+Hg + Co + Ni Supergene Stage	Vargas, 1983 Guillou et al., 1988 Ouguir et al., 1994 Popov, 1995 Baroudi et al., 1999 Levresse, 2001 Tuduri, 2005 Gasquet et al., 2005
Bou Fliou	Bou Teglimt Granodiorite	Disseminated ore and mineralized quartz veins and breccia zones along NE-SW faults	Quartz-chlorite-hematite-dolomite-calcite	Three paragenetic stages Early iron oxide stage Stage: As-Fe Polymetallic stage : Ccp + Gal + Sp + Ag + Bi + Co + Au	This study

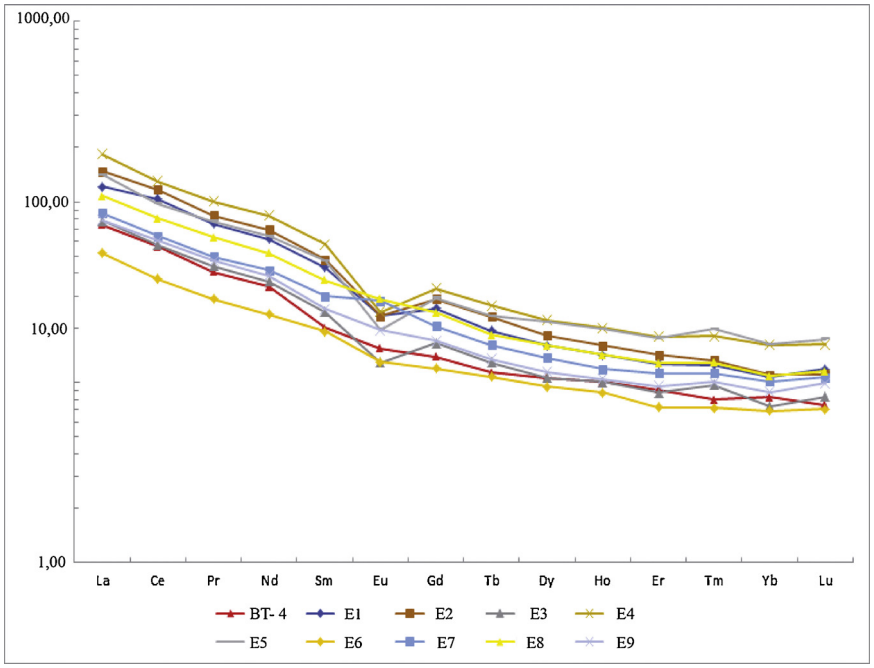

Fig. 20. Chondrite-normalized REE patterns for the selected samples from Bou Fliou mineralized structure; chondrite normalizing values are from Boynton (1984); BT4: sample from Bou Teglimt granodiorite.

Table 7
Main characteristics of IOCG deposits.

IOCG deposits	Host rock	Metal association	Deposit style	Tectonic environments	Hydrothermal alteration	Associated magma	References
Olympic Dam-district (*Olympic Dam deposit)*	Granite	Polymetallic Fe, Cu, Au, Ag, REE	Breccias (one or more stages) Magnetite and hematite matrix	Intracontinental arc	Potassic/ intemediate argilic alteration	Metaluminous oxidized monzodiorite	Creaser (1996) Creaser and Cooper, 1993 Haynes, 2000
Cloncury district (*Osborne and Starra deposits*)	Metasediments	Polymetallic Cu, Au, Ag, Bi, Co, W	Hydrothermal vein and disseminations Breccias	Intracontinental arc	Sodic–calcic widespread	Diorite to monzogranite (Alkaline to subalkaline)	Williams and Pollard, 2003 Pollard et al. (1998) Betts et al. (2003) Mark et al. (2006)
Carajás district (*Salobo, Sossego, deposit*)	Amphibolites, BIFs, metagraywackes and quartzites	Cu-Au (Mo-Ag-U-ETR)	Massive lense of magnetite	Continental margin arc?	Sodic–calcic restricted	Subalkaline (Estrela Granite, Old Salobo pluton)	Holdsworth and Pinheiro (2000) Tallarico et al. (2005) Requia (2002)

base metals, the Bou Fliou deposit can be classified as “Iron Oxides-Copper-Gold deposit”. This new mineralization style described in the Saghro massif can be applied as an exploration tool for discovering future deposits in the whole Anti-Atlas.

Acknowledgements

The authors would like to thank the associate editor Irina Talovina and editor-in-chief Astrid Holzheid for the edition and handling of this research article. The two anonymous reviewers and the Editor-in-chief are greatly acknowledged for their excellent contributions and appreciative comments that helped us to revise and improve this manuscript. This study is part of the PhD thesis of the first author (B.B.). We thank DLGR laboratory (Cadi Ayyad University) and LAGAGE laboratory (Ibn Zohr University) for logistic and funding supports of this project.

References

Abia, E.H., Nachit, H., Marignac, C., Ibhi, A., AÏt Saadi, S., 2003. The polymetallic Au–Ag-bearing veins of Bou Madine (Jbel Ougnat, eastern Anti-Atlas, Morocco): tectonic control and evolution of a Neoproterozoic epithermal deposit. J. Afric. Earth Sci. 36, 251–271.

Aït Malek, H., Gasquet, D., Bertrand, J.M., Leterrier, J., 1998. Géochronologie U–Pb sur zircon de granitoïdes éburnéens et panafricains dans les boutonnières protérozoïques d’Igherm, du Kerdous et du Bas Draa (Anti-Atlas occidental, Maroc). Comptes Rendues Acad. Sci. 327, 819–826 Paris.

Alansari, A., 1997. La mine d’or de Tiouit: un exemple de veines aurifères mésothermales associées à une granodiorite d’âge protérozoïque supérieur (Massif Panafricain du Jbel Saghro, Anti-Atlas, Maroc). Unpublished Ph.D. Thesis. Université Cadi Ayyad, Faculté des Sciences Semlalia, Marrakech, Morocco 284 p.

Alansari, A., Mouguina, M., Maacha, M., 2011. Le gisement de Tiouit à Au-Cu-Ag (Massif Néoprotérozoïque du J. Saghro). In: In: Mouttaqi, A., Rjimati, E.C., Maacha, L., Michard, A., Soulaimani, A., Ibouh, H. (Eds.), Les principales mines du Maroc. Notes et Mémoires du Service Géologique du Maroc, vol 564. pp. 53–57.

Baidada, B., Cousens, B., Alansari, A., Soulaimani, A., Barbey, P., Ilmen, S., Ikenne, M., 2017. Geochemistry and SmeNd isotopic composition of the Imiter Pan-African granitoids (Saghro massif, eastern Anti-Atlas, Morocco): geotectonic implications. J. Afr. Earth Sci. 127, 99–112.

Baidada, B., Ikenne, M., Barbey, P., Soulaimani, A., Cousens, B., Haissen, F. Ilmen, S., Alansari, A., 2018. SHRIMP U–Pb zircon geochronology of the granitoids of the Imiter Inlier: Constraints on the Pan-African events in the Saghro massif, Anti-Atlas (Morocco). Journal of African Earth Sciences, in press.

Bajja, A., 1998. Volcanisme syn à post orogénique du Néoprotérozoïque de l'Anti- Atlas : implications pétrogénétiques et géodynamiques. Doctorat d'Etat Thesis. Université Chouaib Doukkali, El Jadida, Maroc 215 pp.

Barodi, B., Belkasmi, A., Bouchta, R., Qadrouci, A., 1998. Les minéralisations argentifères du Maroc: cas du gisement d'Imiter Vol. 531-532. Chronique de la Recherche Minière, pp. 77–92.

Baroudi, Z., Beraouz, H., Rahimi, A., Saquaque, A., Chouhaidi, M., 1999. Minéralisations polymétalliques argentifères d'Imiter Jbel Saghro, Anti-Atlas, Maroc: minéralogie, évolution des fluides minéralisateurs et mécanismes de dépôts Vol. 536-537. Chronique de la Recherche Minière, pp. 91–112.

Barton, M.D., Johnson, D.A., 1996. Evaporitic- source model for igneous related Fe-oxide (REE– Cu–Au) mineralization. Geology 24, 259–262.

Barton, M.D., Johnson, D.A., 2000. Alternative brine sources for Fe-oxide(-Cu-Au) systems: implications for hydrothermal alteration and metals. In: Porter, T.M. (Ed.), Hydrothermal Iron Oxide Copper-Gold & Related Deposits: A Global Perspective, 1. Australian Mineral Foundation, pp. 43–60.

Barton, M.D., Jensen, E.P., Ducea, M., 2005. Fluid sources for IOCG (Candelaria, punta del Cobre) and porphyry Cu-style mineralization, Copiapó batholith, Chile: geologic and Sr isotopic constraints. Geol Soc Am Abst w Prog 37 (7), 316.

Bastrakov, E.N., Skirrow, R.G., Davidson, G.J., 2007. Fluid evolution and origins of Iron oxide CuAu prospects in the Olympic Dam District, Gawler Craton, South Australia. Econ. Geol. 102, 1415–1440.

Beaudoin, G., Dupuis, C., 2007. Signature géchimique des oxydes de fer et application à l'exploration minière volet. Rapport annuel sous projet SC22.

Benoit, L., 2000. Ore deposits in an ocean-continent subduction context. Projet Consorem 2009-05. pp. 64.

Benziane, F., 2007. Lithostratigraphie et évolution géodynamique de l'Anti-Atlas (Maroc) du Paléoprotérozoïque au Néoprotérozoïque: exemples de la boutonnière de Tagragra de Tata et du Jbel Saghro. PhD thesis. Université de Savoie CISM, Chambéry, France 320 pp.

Betts, P.G., Giles, D., Lister, G.S., 2003. The Hitaba Event—an example of hotspot related flat subduction?: geological Society of Australia. Abstracts 27, 67.

Blein, O., Baudin, T., Ch_evremont, P., Soulaimani, A., Admou, H., Gasquet, D., Cocherie, A., Egal, E., Youbi, N., Razin, Ph, Bouabdelli, M., Gombert, Ph, 2014. Geochronological constraints on the polycyclic magmatism in the Bou Azzer-El Graara inlier (central Anti-Atlas Morocco). J. Afr. Earth Sci. 99, 287–306.

Borisenko, A.S., Borovikov, A.A., Pavlova, G.G., Kalinin, Y.A., Nevolko, P.A., Lebedev, V.I., Maacha, L., Kostin, A.V., et al., 2013. Formation conditions of Hg-silver deposition at the Imiter deposit (Anti-Atlas, Morocco). Johnsson, E. (Ed.), Mineral Deposit Research for a High-Tech World. Proceedings of 12th Biennial SGA Meeting, Uppsala, Sweden 3, 1243–1246.

Bouabdellah, M., Chekroun, F., Alansari, A., Margoum, D., 2016. The granitoid-related tiouit gold deposit, saghro inlier, Eastern Anti-Atlas (Morocco): neoproterozoic mineralization by a polyphase late-magmatic to hydrothermal system. In: Bouabdellah, M., Slack, J.F. (Eds.), Mineral Deposits of North Africa, Mineral Resource Reviews. Springer International Publishing, Switzerland. https://doi.org/10.1007/978-3-319-31733-5.

Boynton, W.V., 1984. Cosmochemistry or the rare earth elements: meteorite studies. In: Henderson, P. (Ed.), Rare Earth Elements Geochemistry. Elsevier, Amsterdam, pp. 63e114.

Camara, L.S., 1993. Cartographie, pétrographie et géochimie des granitoïdes du district minier d'Imiter (Saghro oriental, Anti-Atlas, Maroc).138p. Thèse de 3ème cycle. Université Cadi Ayyad, Marrakech.

Cheilletz, A., Levresse, G., Gasquet, D., Azizi-Samir, M.R., Zyadi, R., Archibald, D.A., Farrar, E., 2002. The giant Imiter silver deposit: neoproterozoic epithermal mineralization in the Anti-Atlas, Morocco: miner. Miner. Depos. 37, 772–781.

Ciobanu, C.L., Cook, N.J., Damian, F., Damian, G., 2006. Gold scavenged by bismuth melts: an example from Alpine shear-remobilizates in the Highiş Massif, Romania Massif, Romania. Mineral. Petrol. 87, 351–384.

Creaser, R.A., 1996. Petrogenesis of a Mesoproterozoic quartz latite-granitoid suite from the Roxby Downs area, South Australia. Precambrian Res. 79, 371–394.

Creaser, R.A., Cooper, J.A., et al., 1993. U-Pb geochronology of middle proterozoic felsic magmatism surronding the olympic dam Cu-U-Au-Ag and moonta Cu-Au-Ag deposits, South Australia. Econ. Geol. 88, 186–197.

Dupuis, C., Beaudoin, G., 2011. Discriminant diagrams for iron oxide trace element of mineral deposit types. Miner. Depos. 46, 319–335.

Ehrig, K., McPhie, J., Kamenetsky, V., 2013. Geology and mineralogical zonation of the Olympic Dam Iron Oxide Cu-U-Au-Ag deposit, South Australia. In: In: Hedenquist, J.W., Harris, M., Camus, F. (Eds.), Geology and Genesis of Major Copper Deposits and Districts of the World: A Tribute to Richard H. Sillitoe 2012. Society of Economic Geologists Special Publication, Littleton, CO, USA, pp. 237–267.

El Baghdadi, M., El Boukhari, A., Jouider, A., Benyoucef, A., Nadem, S., 2003. Calcalkaline arc I-type granitoid associated with S-type granite in the Pan-African belt of eastern Anti-Atlas (Saghro and Ougnat, South Morocco). Gondwana Res. 6, 557–572.

El Hadi, H., Simancas, F., Martìnez-Poyatos, J., Azor, A., Tahiri, A., Montero, P., Fanning, C.M., Bea, F., Gonz_alez-Lodeiro, F., 2010. Structural and geochronological constraints on the evolution of the Bou AzzerNeoproterozoic ophiolite (Anti-Atlas, Morocco). Precambrian Res. 182, 1–14.

Ennih, N., Liégeois, J.P., 2001. The Moroccan Anti-Atlas: the West African craton passive margin with limited Pan-African activity. Implications for the northern limit of the craton. Precambrian Res. 112, 291–304.

Ennih, N., Liégeois, J.P., 2008. The Boundaries of the West African Craton, With Special Reference to the Basement of the Moroccan Metacratonic Anti-atlas Belt. Special Publications 2008, 297. Geological Society, London, pp. 1–17.

Errami, E., Bonin, B., Laduron, D., Lasri, L., 2009. Petrology and geodynamic significance of the post-collisional Pan-African magmatism in the Eastern Saghro area (Anti-Atlas, Morocco). J. Afr. J. Earth Sci. 55, 105–124.

Essarraj, S., Boiron, M.C., Cathelineau, M., Tarantola, A., Leisen, M., Boulvais, Ph., Maacha, L., 2017. Basinal Brines at the origin of the imiter Ag-Hg deposit (Anti-Atlas, Morocco): evidence from LA-ICP-MS data on fluid inclusions, halogen signatures, and stable isotopes (H, C, O). Econ. Geol. 111, 1753–1781. https://doi.org/10.2113/econgeo.111.7.1753.

Fekkak, A., Pouclet, A., Badra, L., 2002. The pre-Pan-African rifting of Saghro (Anti- Atlas, Morocco): example of the middle neoproterozoic basin of Boumalne. Bulletin de la Société Géolpgique de France 173 (1), 25–35.

Foster, D.A., Schafer, C., Fanning, C.M., Hyndman, D.W., 2001. Relationships between crustal partial melting, plutonism, orogeny, and exhumation : Idaho-Bitterroot batholith. Tectonophysics 342, 313–350.

Gaouzi, A., Maacha, L., Ennaciri, A., Gmira, A., Maamar, B., Zouhair, M., Saquaque, A., 2011. Mine d'argent d'Imiter (Anti-Atlas oriental, Maroc). In: In: Michard, A., Saddiqi, O., Chalouan, A., Rjimati, E.C., Mouttaqi, A. (Eds.), Nouveaux guides géologiques et miniers du Maroc e Volume 9, Les principales mines du Maroc. Notes et Mémoires du Service Géologique du Maroc, vol. 564. pp. 45–52.

Gasquet, D., Levresse, G., Cheilletz, A., Azizi-Samir, M.R., Mouttaqi, A., 2005. Contribution to a geodynamic reconstruction of the Anti-Atlas (Morocco) during Pan-African times with the emphasis on inversion tectonics and metallogenic activity at the Precambrian-Cambrian transition. Precambrian Res. 140, 157–182.

Gasquet, D., Ennih, N., Li_egeois, J.P., Soulaimani, A., Michard, A., 2008. The Pan-African belt. In: In: Michard, A., Saddiqi, O., Chalouan, A., Frizon de Lamotte, D. (Eds.), Continental Evolution: the Geology of Morocco. Lecture Notes in Earth Sciences, vol. 116. pp. 33–64.

Grappe, J., 1974. Les gîtes sulfurés de remaniement supergène (oxydation, cémentation). Rapport interne CG.G.M., Ecole des mines de Paris.

Guilllou, J.J., Montilel, J., et Samama, Jc, 1981. Etude des minéralisations de la mine d'lmiter (Maroc). B.R.P.M.-E.N.S.G. Rapport interne.

Guillou, J.J., Monthel, J., Samama, J.C., Tijani, A., 1988. Morphologie et chronologie relative des associations minérales du gisement mercuro-argentifère d'Imiter (Anti-Atlas, Maroc). Notes et Mémoires du Service Géologique du Maroc 334, 215–228.

Haynes, D.W., 2000. Iron oxide copper (-gold) deposits: their position in the ore deposit spectrum and modes of origin. In: In: Porter, T.M. (Ed.), Hydrothermal Iron Oxide Copper-Gold and Related Deposits a Global Perspective, 1: Adelaide, Australian Mineral Foundation v. 1. pp. 71–90.

Hefferan, K., Soulaimani, A., Samson, S.D., Admou, H., Inglis, J., Saquaque, A., Heywood, N., 2014. A reconsideration of Pan African orogenic cycle in the Anti- Atlas Mountains, Morocco. J. Afr. Earth Sci. 98, 34–46.

Hindermeyer, J., Gauthier, H., Destombes, J., Choubert, G., Faure-Muret, A., Laville, E., Lesage, J.L., du Dresnay, R., 1977. Carte géologique au 1/200 000, Jebel Saghro-Dadès (Haut Atlas central, sillon Sud-Atlasique et Anti-Atlas oriental) 161 Notes et Mémoires du Service Géologique du Maroc.

Hitzman, M.W., Oreskes, N., Einaudi, M.T., et al., 1992. Geological characteristics and tectonic setting of Proterozoic iron oxide (Cu-U-Au-LREE) deposits. Precambrian Res. 58, 241–287.

Holdsworth, R., Pinheiro, R.V.L., 2000. The anatomy of shallow-crustal transpressional structures: insights from the Archean Carajás fault zone, Amazon, Brazil. J. Struct. Geol. 22, 1105–1123.

Ighid, L., Saquaque, A., Reuber, I., 1989. Plutons syn-cinématiques et la déformation panafricaine majeure dans le Saghro oriental (boutonnière d'Imiter, Anti-Atlas, Maroc) 309. C. R. Acad. Sci., Paris, pp. 615–620 (II).

Ilmen, S., Alansari, A., Bajddi, A., Maacha, L., 2015. Cu–Au vein mineralization related to the Talat n'Imjjad shear zone (western High Atlas, Morocco): geological setting, ore mineralogy, and geochemical evolution. Arab. J. Geosci. 8, 5039–5056. https://doi.org/10.1007/s12517-014-1503-y.

Leistel, J.M., Qadrouci, A., 1991. Le gisement argentifèe d'Imiter (Protérozoïque supérieur de l'Anti-Atlas, Maroc). Contrôles des minéralisations, hypothèse génétique et perspectives pour l'exploration 502. Chronique de la Recherche Minnière, pp. 5–22.

Levresse, G., 2001. Contribution à l'établissement d'un mode génétique des gisements d'Imiter (Ag-Hg), Bou Madine (Pb-Zn-Cu-Ag-Au) et Bou Azzer (Co-Ni-As-Au-Ag) dans l'Anti-Atlas marocain. Unpublished PhD Thesis. INPL, Nancy, France.

Levresse, G., Cheilletz, A., Gasquet, D., Reisberg, L., Deloule, E., Marty, B., Kyser, K., 2004. Osmium, sulphur and helium isotopic results from the giant Neoproterozoic epithermal Imiter silver deposit, Morocco: evidence for a mantle source. Chem. Geol. 207, 59–79.

Levresse, G., Bouabdellah, M., Cheilletz, A., Gasquet, D., Maacha, L., Tritlla, J., Banks, D., Azizi Samir, M.R., 2016. Degassing As the Main Ore-forming Process at the Giant Imiter Ag–Hg Vein Deposit in the Anti-atlas Mountains, Morocco. Mineral Deposits of North Africa, Mineral Resource Reviews. https://doi.org/10.1007/978-3-319-31733-5_2.

Lydon, J.W., 2007. An overview of the economic and geological contexts of Canada's major mineral deposit types. Dans. In: Goodfellow, W.D. (Ed.), Mineral Deposits of Canada: A Synthesis of Major Deposit-Types, District Metallogeny, the Evolution of Geological Provinces, and Exploration Methods. Association Géologique du Canada, Division des Gîtes Minéraux, Publication Spéciale No. 5, pp. 3–48.

Mark, G., Oliver, N.H.S., Carew, M.J., 2006. Insights into the genesis and diversity of epigeneticCu– Au mineralisation in the Cloncurry district, Mt Isa Inlier, northwest Queensland. Aust. J. Earth Sci. 53, 109–124.

Massironi, M., Bertoldi, L., Calafa, P., Visonà, D., Bistacchi, A., Giardino, C., Schiavo, A.,

2008. Interpretation and processing of ASTER data for geological mapping and granitoids detection in the Saghro massif (eastern Anti-Atlas, Morocco). Geosphere 4, 736–759.
Michard, A., Frizon de Lamotte, D., Saddiqi, O., Chalouan, A., 2008a. An outline of the geology of Morocco. In: Michard, A., Saddiqi, O., Chalouan, A., Frizon de Lamotte, D. (Eds.), Continental Evolution: The Geology of Morocco. Lecture Notes in Earth Sciences 116. Springer-Verlag, Berlin Heidelberg, pp. 1–31 Chapter 1.
Michard, A., Hoepffner, C., Soulaimani, A., Baidder, L., 2008b. The Variscan belt. In: In: Michard, A., Saddiqi, O., Chalouan, A., Frizon de Lamotte, D. (Eds.), Continental Evolution: The Geology of Morocco. Lecture Notes in Earth Sciences, vol. 116. Springer-Verlag, Berlin Heidelberg, pp. 65–132 Chapter 3.
Monteiro, L.V.S., Xavier, R.P., Hitzman, M.W., Juliani, C., Souza Filho, C.R., Carvalho, E.R., 2008. Mineral chemistry of ore and hydrothermal alteration at the Sossego iron oxide–copper–gold deposit, Carajás Mineral Province, Brazil. Ore Geol. Rev. 34, 317–336.
Moreto, C.P.N., Monteiro, L.V.S., Xavier, R.P., Creaser, R.A., DuFrane, A., Melo, G.H.C., Silva, M.A.D., Tassinari, C.C.G., Sato, K., 2014. Timing of multiple hydrothermal events in the iron oxide-copper-gold deposits of the Southern copper belt, Carajás province, Brazil: Mineralium Deposita. Morocco. Keyworth. Nottingham Br. Geol. Surv. 324.
Nisbet, B., Cooke, J., Richards, M., Williams, C., 2000. Exploration for iron oxide copper gold deposits in Zambia and Sweden: comparison with the Australian experience. In: In: PORTER, T.M. (Ed.), Hydrothermal Iron Oxide Copper–Gold & Related Deposits: A Global Perspective, vol. 1. Australian Mineral Foundation, Adelaide, pp. 297–308.
O'Connor, E.A., Barnes, R.P., Beddoe-Stephens, B., Fletcher, T., Gillespie, M.R., Hawkins, M.P., Loughlin, S.C., Smith, M., Smith, R.A., Waters, C.N., Williams, M., 2010. Geology of the Drâa, Kerdous, and Boumalne Districts, Anti-atlas.
Ouguir, H., Macaudi_ere, J., Dagallier, G., Qadrouci, A., Leistel, J.M., 1994. Cadre structural du gîte Ag-Hg d'Imiter (Anti Atlas, Maroc); implication métallogénique. Bulletin de la Société Géologique de France 165, 233–248.
Ouguir, H., Macaudière, J., Dagallier, G., 1996. Le Protérozoïque supérieur d'Imiter, Saghro oriental, Maroc : un contexte géodynamique d'arrière-arc. J. Afr. Earth Sci. 22, 173–189.
Paile, Y., 1983. Etude des séries volcaniques du Précambrien III de l'Ougnat (AntiAtlas oriental, Maroc) et des minéralisations plombo-zincifères complexes associées (gîte de Bou Madine). Unpublished PhD Thesis. Université de Paris XIOrsay, France 145 pp.
Pollard, P.J., 2000. Evidence of a magmatic fluid and metal source for Fe-oxide Cu–Au mineralization. In: In: Porter, T.M. (Ed.), Hydrothermal Iron Oxide Copper–Gold and Related Deposits: a Global Perspective, vol 1. PGC, Adelaide, pp. 27–41.
Pollard, P.J., 2006. An intrusion-related origin for Cu–Au mineralization in iron oxide–-copper–gold (IOCG) provinces. Miner. Depos. 41, 179–187.
Pollard, P.J., Mark, G., Mitchell, L.C., 1998. Geochemistry of post-1540 ma granites in the Cloncurry district, Northwest Queensland. Econ. Geol. 93, 1330–1334.
Popov, A.G., 1995. Gisement argentifère d'Imiter : Etude minéralogique paragenèse et zonalité du gisement. Rapport interne SMI. pp. 62.
Requia, K., 2002. The Archean Salobo Iron Oxide Copper–gold Deposit, Caraja´s Mineral Province. University of Geneva, Brazil PhD Thesis.
Schiavo, A., Taj Eddine, K., Algouti, A.H., Benvenuti, M., Dal Piaz, G.V., Eddebbi, A., El Boukhari, A., Laftouhi, N., Massironi, M., Moratti, G., Ouanaimi, H., Pasquaré, G., Visonà, D., 2007. Notice explicative, Carte Géologique du Maroc au 1/50.000, feuille d'Imiter. Notes et Mémoire Service Géologique, Maroc. 518 bis. pp. 1–96.
Soulaimani, A., Michard, A., Ouanaimi, H., Baidder, L., Raddi, Y., Saddiqi, O., Rjimati, E.C., 2014. Late Ediacaran-Cambrian structures and their reactivation during the Variscan and Alpine cycles in the Anti-Atlas (Morocco). J. Afr. Earth Sci. 98, 94–112.
Tallarico, F.H.B., Figueiredo, B.R., Groves, D.I., Kositcin, N., McNaughton, N.J., Fletcher, I.R., Rego, J.L., 2005. Geology and SHRIMP U-Pb geochronology of the Igarapé Bahia deposit, Carajás copper-gold belt, Brazil: an Archean (2.57 Ga) example of iron-oxide Cu-Au-(U-REE) mineralization. Econ. Geol. 100, 7–28.
Thomas, R.J., Chevallier, L.P., Gresse, P.G., Harmer, R.E., Eglington, B.M., Armstrong, R.A., de Beer, C.H., Martini, J.E.J., de Kock, G.S., Macey, P.H., Ingram, B.A., 2002. Precambrian evolution of the Sirwa window, Anti-Atlas Orogen, Morocco. Precambrian Res. 118, 1–57.
Thomas, R.J., Fekkak, A., Ennih, N., Errami, E., Loughlin, S.C., Gresse, P.G., Chevallier, L.P., Liégeois, J.P., 2004. A new lithostratigraphic framework for the Anti-Atlas Orogen, Morocco. J. Afr. Earth Sci. 39 (3), 217–226.
Toummite, A., Liégeois, J.P., Gasquet, D., Bruguier, O., Beraaouz, E.H., Ikenne, M., 2012. Field, geochemistry and Sr-Nd isotopes of the Pan-African granitoids from the Tifnoute Valley (Sirwa, Anti-Atlas; Morocco): a post-collisional event in a metacratonic setting. Mineral. Petrol. 107 (5), 1–25.
Tuduri, J., 2005. Processus de formation et relations spatio-temporelles des minéralisations à or et argent en contexte volcanique Précambrien (Jbel Saghro, Anti-Atlas, Maroc) implications sur les relations déformation-magmatisme volcanisme-hydrothermalisme. Université D'Orléans, Thèse 3ème cycle.
Tuduri, J., Chauvet, A., Ennaciri, A., Barbanson, L., 2005. Model of formation of the Imiter silver deposit (eastern Anti-Atlas, Morocco): new structural and mineralogical constraints. Comptes Rendus Géosci. 338, 253–261.
Vargas, J.M., 1983. Etude métallographique des minéralisations mercuroargentifères d'Imiter. Fondation Scientifique de la Géologie et de ses applications, Nancy, pp. 60.
Walsh, G.J., Aleinikoff, J.N., Benziane, F., Yazidi, A., Armstrong, T.R., 2002. U-Pb zircon geochronology of the Paleoproterozic Tagragra de Tata inlier and its Neoproterozoic cover, western Anti-Atlas, Morocco. Precambrian Res. 117, 1–20.
Walsh, G.J., Benziane, F., Aleinikoff, J.N., Harrison, R.W., Yazidi, A., Burton, W.C., Quick, J.E., Saadane, A., 2012. Neoproterozoic tectonic evolution of the Jebel Saghro and Bou Azzer-El Graara inliers, eastern and central Anti-Atlas, Morocco. Precambrian Res. 216, 23–62.
Williams, P.J., 2010. Classifying IOCG Deposits. In: Exploring for Iron Oxide Copper–Gold Deposits: Canada and Global Analogues 20. Geological Association of Canada, Short Course Notes, pp. 11–19.
Williams, P.J., Pollard, P.J., 2003. Australian Proterozoic iron oxide CuAu deposits: an overview with new metallogenic and exploration data from the Cloncurry districtp, northwest Queensland. Exploration Mining Geol. 10, 191–213.
Williams, P.J., Barton, M.D., Johnson, D.A., Fontboté, L., DeHaller, A., Mark, G., Oliver, N.H.S., Marschik, R., 2005. Iron oxide copper-gold deposits: geology, space-time distribution, and possible mode of origin. Dans. In: Hedenquist, J.W., Thompson, J.F.H., Goldfarb, R.J., Richards, J.P. (Eds.), Economic Geology 100th Anniversary Volume: Society of Economic Geologists, pp. 371–405.